Characterization of sequence determinants of enhancer function using natural genetic variation

Marty G. Yang,[1,2,*] Emi Ling,[1,3,*] Christopher J. Cowley,[1,4] Michael E. Greenberg,[1,#] and Thomas Vierbuchen[5,6,#,‡]

[1] Department of Neurobiology, Harvard Medical School, Boston, MA, USA

[2] Program in Neuroscience, Harvard Medical School, Boston, MA, USA

[3] Present Address: Department of Genetics, Harvard Medical School, Boston, MA, USA

[4] Present Address: Laboratory of Mammalian Cell Biology and Development, Howard Hughes Medical Institute, The Rockefeller University, New York, NY, USA

[5] Developmental Biology Program, Sloan Kettering Institute for Cancer Research, New York,
NY, USA

[6] Center for Stem Cell Biology, Sloan Kettering Institute for Cancer Research, New York,
NY, USA

[*] These authors contributed equally

[#] Correspondence: meg@hms.harvard.edu and vierbuct@mskcc.org

[‡] Lead Contact

ABSTRACT

Sequence variation in enhancers that control cell type-specific gene transcription contributes significantly to phenotypic variation within human populations. However, it remains difficult to predict precisely the effect of any given sequence variant on enhancer function due to the complexity of DNA sequence motifs that determine transcription factor (TF) binding to enhancers in their native genomic context. Using F_1-hybrid cells derived from crosses between distantly related inbred strains of mice, we identified thousands of enhancers with allele-specific TF binding and/or activity. We find that genetic variants located within the central region of enhancers are most likely to alter TF binding and enhancer activity. We observe that the AP-1 family of TFs (Fos/Jun) are frequently required for binding of TEAD TFs and for enhancer function. However, many sequence variants outside of core motifs for AP-1 and TEAD also impact enhancer function, including sequences flanking core TF motifs and AP-1 half sites. Taken together, these data represent one of the most comprehensive assessments of allele-specific TF binding and enhancer function to date and reveal how sequence changes at enhancers alter their function across evolutionary timescales.

INTRODUCTION

Genome sequencing efforts have uncovered large numbers of sequence variants associated with phenotypic variation in complex traits in human populations. A significant proportion of these genetic variants occur within the ~2-3 x 10^6 *cis*-regulatory elements (CREs) predicted across the human genome (Carroll 2008; Maurano *et al*., 2012; Pickrell 2014; Li *et al*., 2016; Boyle *et al*., 2017). The majority of these CREs are thought to be gene-distal enhancers that potentiate gene transcription in a cell type- or cell state-specific manner (Keilwagen *et al*., 2019). However, pinpointing the specific sequence changes in CREs that impact expression of linked genes, and downstream molecular and cellular phenotypes, remains a critical challenge in the field (Farh *et al*., 2015; Nasser *et al*., 2021; Lapppalainen and MacArthur, 2021). More specifically, it is difficult to reliably distinguish functional sequence variants at CREs among a large excess of neutral variants. As a result, functional assays, such as plasmid-based reporters, have typically been used to assess the impact of individual sequence variants within enhancers. Since these experiments can be laborious to perform and subject to experimental artifacts, a better method for defining sequence-to-function relationships for enhancers in their endogenous genomic context could have a transformative effect on our ability to identify functional sequence variants in CREs in human genomes (Klein *et al*., 2020; Levo and Segal, 2014).

Enhancers are typically bound by ~4-5 TFs that specifically recognize short sequence motifs (~6-12 nucleotides; Bilu and Barkrai, 2005; Meuleman *et al*., 2020). TFs function as adaptor proteins to recruit transcriptional regulatory complexes to

enhancers, leading to potentiation of transcription at associated gene promoters. Enhancer activity is highly cell type-specific, and this specificity of function is encoded by the type and arrangement (also known as regulatory grammar) of TF-binding motifs within each enhancer (Zeitlinger 2020; Jindal and Farley 2021). Enhancers that control transcription in specific cell types are often bound by combinations of TFs that occur uniquely in that cellular context (Spitz and Furlong, 2012; Wei *et al*., 2018). This complicates efforts to identify generalizable features that can be used to prioritize enhancer sequence variants *in silico* (Kasowski *et al*., 2010; Ding *et al*., 2014; Tehranchi *et al*., 2016).

Although enhancers cannot be defined by a singular set of sequence features, they do exhibit stereotyped chromatin features that can be measured genome-wide, such as chromatin accessibility (controlled by TF and co-factor binding), histone post-translational modifications (e.g. H3K4me1/2 and H3K27ac), and bi-directional transcription of short enhancer RNAs (Heintzman *et al*., 2007; Boyle *et al*., 2008; Creyghton *et al*., 2010; Kim *et al*., 2010; Rada-Iglesias *et al*., 2011). These chromatin signatures have been used extensively to identify millions of putative enhancers in a wide range of cell types and across different stages of organismal development (Kundaje *et al*., 2015). While mapping genomic regions that function as enhancers has facilitated the identification of DNA-binding motifs enriched at enhancers in different cell types, these data have not proven to be sufficient to generate quantitative, predictive models for TF binding and enhancer function from available databases of enhancer sequences (Deplancke *et al*., 2016).

Sequence variants that disrupt TF binding can be highly informative for identifying sequences critical for the control of enhancer function in specific cell types (Wittkopp and Kalay, 2011; Albert and Kruglyak, 2015; Lappalainen 2015; Pai *et al*., 2015; Vierbuchen *et al*., 2017). Our lab and others have previously used the extensive genetic variation present among inbred mouse strains to conduct "mutagenesis screens" of enhancer sequences in their native chromatin context (Heinz *et al*., 2013; Vierbuchen *et al*., 2017; Wong *et al*., 2017; van der Veeken *et al*., 2019). By crossing highly divergent inbred mouse strains to generate F_1 hybrids, it is possible to directly compare the activity of two alleles of each enhancer locus within the same cellular environment.

Using mouse embryonic fibroblasts (MEFs) derived from two distinct inbred strains, we found that the binding of AP-1 TFs is required for chromatin accessibility and activity at many active enhancers in fibroblasts (Vierbuchen *et al*., 2017). However, we also observed that many instances of allele-specific AP-1 binding cannot be readily explained by sequence variants within AP-1 motif(s). These data indicated that, at many enhancer loci, sequence features outside of AP-1 TF-binding sites contribute to AP-1 binding. In this previous study, we observed an enrichment of variants in motifs for putative collaborating TFs (e.g. TEAD) at these sites, but the nature of this collaborative relationship with AP-1 remained to be defined. Both AP-1 and TEAD are broadly expressed and have critical roles in mediating signal-dependent transcription downstream of the Ras/MAPK and Hippo/YAP/TAZ pathways, respectively. Consistent

with our findings, the co-occurrence of AP-1 and TEAD motifs at enhancers has also been noted in a variety of human tumor cells, providing support for the idea that AP-1 and TEAD coordinately regulate cell fate and proliferation. Nevertheless, further delineation of the sequence features that determine the binding of AP-1 and TEAD TFs to enhancers, and whether the binding of one of these TFs is dependent on the other, could provide insight into enhancer function across a broad range of cellular contexts (Zanconato *et al*., 2015).

In the present study, we carried out an extensive allele-specific analysis of chromatin state (ATAC-seq, H3K27ac, H3K4me1/2, and H3K4me3) and TF binding (Fos, Tead1, and CTCF) in F_1-hybrid MEFs derived from crosses between C57BL/6J mice and a panel of nine inbred mouse lines, including several wild-derived inbred strains from distinct sub-species of mice that contain a high frequency of SNPs/indels (1 in every ~85-170 bp) compared to C57BL/6J mice. Using these genetically divergent strains, we examined the frequency and distribution of SNPs/indels at thousands of enhancers with allele-specific chromatin features and/or TF binding patterns. We found that sequence variants within the central ~50 bp of enhancer sequences were most likely to lead to an allele-specific change in enhancer activity. These data also revealed that AP-1 binding is often required for TEAD TF binding to enhancers, whereas TEAD is generally not required for AP-1 TF binding. This result is consistent with a model in which AP-1 TFs function as pioneer factors to facilitate binding of additional TFs and to enable enhancer selection in fibroblasts. An analysis of our allele-specific data revealed that additional sequence features, such as partial AP-1 motifs and nucleotide

sequences flanking core AP-1 binding motifs, also contribute to enhancer function. These findings provide new insight into how AP-1 TFs function at enhancers in fibroblasts, and suggest that across other cell types, AP-1 TFs may employ similar collaborative binding mechanisms at enhancers. In addition, our data provide new insight into the crosstalk between Ras/MAPK and Hippo/YAP/TAZ/TEAD signal-dependent gene expression and suggest that Ras/MAPK-induced AP-1 can play an instructive role in determining the output of Hippo/YAP/TAZ/TEAD-dependent transcriptional programs.

RESULTS

Mapping TF binding and CREs in F_1-hybrid MEFs

To identify genetic variants that modulate TF binding and/or chromatin state at CREs, we isolated MEFs from male F_1-hybrid embryos derived from crosses between C57BL/6J females and males from nine distinct inbred mouse strains, including four wild-derived inbred strains (CAST/EiJ, MOLF/EiJ, PWK/PhJ, and SPRET/EiJ) that have a high frequency of SNPs/indels compared to C57BL/6J mice (**Figure 1A**; **Supplementary File 1**). Genome sequencing data is available for each inbred strain, meaning that we can query up to ten distinct alleles at each CRE sequence for differences in TF binding and/or *cis*-regulatory activity (Keane *et al*., 2011). To identify potential differences in CRE function that result from sequence variants between maternal (C57BL/6J) and paternal chromosomes, we generated the following allele-specific datasets from the four wild-derived inbred F_1-hybrid strains: chromatin features

associated with *cis*-regulatory function (ATAC-seq, H3K4me1/2, H3K4me3, and H3K27ac), occupancy of TFs that bind many CREs in fibroblasts (Fos and Tead1), putative insulator elements (CTCF), and gene transcription levels (chromatin-associated RNA-seq; **Figure 1B-F, Figure 1 – figure supplement 1A; Supplementary File 2**). For the remaining F_1-hybrid lines (129S1/SvImJ, A/J, BALB/cJ, DBA/2J, and NOD/ShiLtJ), we only performed CUT&RUN for Fos and H3K27ac (**Supplementary File 2**). H3K27ac Hi-ChIP was also performed in C57BL/6J MEFs to link active enhancers to putative target genes and to other active CREs (**Supplementary File 3**). All experiments were conducted under two distinct conditions: (1) MEFs that were growth arrested in G_0 by serum starvation and (2) serum-starved MEFs that were re-stimulated with serum for 90 minutes. These defined conditions reduce technical variability between samples by synchronizing cells in the population at a specific stage of the cell cycle and allow us to measure the binding of TFs that are induced by serum stimulation, such as AP-1 TFs, at the peak of their activity (Vierbuchen *et al*., 2017).

From each of the two alleles in F_1-hybrid lines, we identified putative primed CREs (ATAC-seq summits that lack H3K27ac) and active CREs (ATAC-seq summits overlapping H3K27ac peaks) (**Figure 1 – figure supplement 2A**). For all active CREs, we classified sites as either gene-proximal (promoters) or gene-distal (putative enhancers) based on their distance to the nearest annotated TSS (**Figure 1 – figure supplement 2C**). In total, we found 76,517 unique genomic loci defined as active CREs from the nine F_1 hybrids surveyed, and 50.4% of allele pairs at these sites harbor SNP(s) within +/- 60 bp of the ATAC-seq summit used to define each enhancer locus.

185

186 **Identification of allele-specific CREs in F_1-hybrid MEFs**

187 In aggregate, across all nine F_1-hybrid lines, 24.4% of pairs of active enhancer
188 alleles on autosomes show a statistically significant difference in H3K27ac levels
189 between maternal (C57BL/6J) and paternal alleles (**Figure 1C, Figure 1 – figure**
190 **supplement 2B**). Among these allele-specific sites, 56.2% and 15.3% exhibit a >2-fold
191 and >4-fold difference in H3K27ac signal, respectively. To determine whether
192 differences in H3K27ac between alleles are associated with changes in transcription of
193 the gene that they regulate, we first identified high-confidence enhancer-TSS
194 interactions using H3K27ac Hi-ChIP data, and then examined whether transcription of
195 the linked gene was higher on the chromosome with the active enhancer allele. We
196 found that allele-specific enhancers are more likely to interact with genes that exhibit
197 allele-specific transcriptional differences than enhancers that have similar levels of
198 H3K27ac on each allele (14.5% and 9.1% of active enhancers with detectable H3K27ac
199 Hi-ChIP loops with an active promoter, respectively; **Figure 1 – figure supplement**
200 **2D**). This suggests that allele-specific differences in H3K27ac are indicative of
201 functional differences in the transcriptional regulatory activity of enhancers, consistent
202 with findings from previous studies (Creyghton *et al*., 2010; Arnold *et al*., 2013; Fulco *et*
203 *al*., 2019).

204

205 Compared to H3K27ac levels at enhancers, levels of promoter-associated
206 histone modification H3K4me3 (3.6%) and gene-distal binding of CTCF (2.6%) are less
207 likely to exhibit significant differences between alleles (**Figure 1D-E**). These data are

consistent with previous studies suggesting that promoters and CTCF-binding sites are more likely to be functionally conserved than enhancers when compared across groups of distantly related species (Schmidt *et al*., 2012; Villar *et al*., 2015; Fudenberg and Pollard, 2019). Furthermore, for each class of active CREs, we found that the frequency of sites with allele-specific H3K27ac signal is proportional to the frequency of SNPs between maternal and paternal alleles (**Supplementary File 4**). We noted that the number of genes with an allele-specific skew in expression level per strain also scaled with the total number of SNPs/indels relative to C57BL/6J in the given strain (**Figure 1 – figure supplement 1B**; **Supplementary File 5**).

Identification of sequence features that impact enhancer selection and activation

Several mechanisms have been proposed for how TFs initially bind enhancers leading to enhancer activation and the expression of genes that were previously silent. It remains unclear whether TF binding is sufficient to displace histone octamers at nucleosomal enhancers or if TF-mediated recruitment of additional co-regulatory proteins, such as chromatin remodeling complexes, is also required (Lidor-Nili *et al*., 2011; Paakinaho *et al*., 2017; Johnson *et al*., 2018). For instance, it is thought that H3K4me1/2 deposition is indicative of enhancers that have been partially activated or primed (Heintzman *et al*., 2007). However, it is not known whether the majority of these primed sites only become active later in development (i.e. subsequently gain H3K27ac; Creyghton *et al*., 2010; Rada-Iglesias *et a*l., 2011; Bonn *et al*., 2012; Bogdanovic *et al*., 2012), or if they typically are fully activated in a single step (i.e. concurrently gain H3K4me1/2 and H3K27ac), such as upon the binding of signal-dependent TFs or during

231 cellular differentiation (Kaikkonen *et al*., 2013; Ostuni *et al*., 2013). To address these
232 hypotheses, we examined our allele-specific H3K4me1 and H3K4me2 ChIP-seq
233 datasets, which contain thousands of allele pairs that have significant differences in
234 these histone modifications (**Figure 1F**). Our previous work suggested that disruption of
235 AP-1 TF binding results in the loss of histone marks associated with both primed and
236 active enhancers (Vierbuchen *et al*., 2017), but whether this feature is generally
237 applicable for all enhancers (independent of AP-1 binding) and whether there are
238 mutations that inactivate enhancers without affecting H3K4me1/2 levels were
239 unresolved. To assess whether the priming and activation of enhancers are genetically
240 separable processes, we focused on H3K4me1/2 levels at enhancers with the greatest
241 difference in H3K27ac levels between alleles. We observed that 70.1% of enhancers in
242 the top decile of allele-specific enhancers have a significant and >2-fold concordant loss
243 of H3K4me1 on the inactive allele, compared to 0.6% of the bottom decile of allele-
244 specific enhancers (peaks with the smallest, statistically significant fold changes in
245 H3K27ac levels between alleles). Chromatin accessibility and AP-1 binding exhibit
246 similar changes to H3K4me1 at enhancers with strongly allele-specific H3K27ac
247 (**Figure 1G**). Together, these data reveal that few if any SNPs/indels cause a significant
248 loss of enhancer H3K27ac and maintain strong enrichment of H3K4me1/2 and
249 chromatin accessibility. Thus, our data is consistent with a model in which enhancer
250 priming/selection and activation are not separable steps mediated by distinct TF-binding
251 events at enhancers in MEFs.
252
253 **Contribution of *cis*- and *trans*-acting effects on enhancer activity**

In F_1 hybrids, both enhancer alleles are exposed to the same nucleoplasmic environment, and thus observed differences between the two alleles are generally considered to be caused directly by local SNPs (i.e. SNPs within the ~200 bp sequence of chromatin accessibility at the CRE in question). However, each enhancer allele is also located within a *cis*-regulatory unit or topologically associated domain (TAD), which contains additional genetic changes outside of the enhancer itself that could potentially impact TF binding or chromatin state at the enhancer in an allele-specific manner (Kilpinen *et al*., 2013; Grubert *et al*., 2015). These "locus-scale" *cis*-acting mechanisms could include: (1) sequence variants in other CREs at the same locus that interact with an enhancer in 3D, (2) gains or losses in CTCF-binding sites that influence 3D interactions between CREs within the *cis*-regulatory unit associated with that enhancer, (3) structural variants that disrupt the organization of the locus such that the enhancer is subject to different 3D interactions, and (4) variation in repeat elements (e.g. LINEs, SINEs) within the locus that are not generally well annotated in genomic datasets (Ou *et al*., 2019). Another possible explanation for allele-specific activity of CREs is parent-of-origin specific imprinting. We excluded CREs at known imprinted loci from subsequent analyses due to the differing nature of this type of allele-specific transcriptional regulation.

To quantify the relative impact of these *cis*-acting, locus-level mechanisms, we analyzed sequencing reads from our allele-specific histone modification datasets, which typically flank the functional CRE sequence and can thus be mapped to one allele or the other even when there are no SNPs present in the accessible chromatin window at

277 enhancers (**Figure 2A, Figure 2 – figure supplement 1B**). We reasoned that
278 enhancers lacking SNPs/indels should only show an allelic skew in H3K27ac levels
279 when these aforementioned non-local mechanisms significantly contribute to the
280 function of those enhancers. Only 9.1% of enhancers that have no SNPs/indels in their
281 central 150 bp (centered on the ATAC-seq summit used to initially define the CRE)
282 exhibit a significant, allele-specific, >2-fold skew in H3K27ac levels on flanking
283 nucleosomes, compared to 22.1% of enhancers with SNPs/indels (**Figure 2F**). This
284 result suggests that it is relatively rare for SNPs outside the enhancer sequence itself to
285 influence the function of the enhancer in question. In addition, allele-specific 0-SNP
286 enhancers are not situated significantly closer (than H3K27ac-matched shared 0-SNP
287 enhancers) to an allele-specific CTCF peak (**Figure 2 – figure supplement 1A, 1C**),
288 suggesting that rearrangement of CTCF-dependent TAD boundaries is not a major
289 contributor to allele-specific differences in enhancer activity at these sites. However,
290 among 0-SNP enhancers, those with allele-specific H3K27ac signal were more likely to
291 be located near another allele-specific enhancer that has at least one SNP/indel
292 (median = 48,623 bp and 75,664 bp for allele-specific and shared 0-SNP enhancers,
293 respectively; **Figure 2 – figure supplement 1D**). In contrast, allele-specific and shared
294 0-SNP enhancers did not exhibit significant differences in their proximity to active CREs
295 in general (**Figure 2 – figure supplement 1E**). Consistent with these findings, we
296 observed that allele-specific 0-SNP enhancers are frequently located in enhancer
297 clusters with another allele-specific enhancer (within ~1-2 kb apart). In such cases, it is
298 difficult to rule out the possibility that the quantification of H3K27ac-marked
299 nucleosomes flanking the 0-SNP enhancer is not simply detecting diffuse signal from

other enhancer(s) in the cluster (**Figure 2B**). Furthermore, based on H3K27ac Hi-ChIP, we rarely observed 0-SNP allele-specific enhancers connected via a long-range loop (e.g. >10 kb) with another allele-specific SNP/indel-containing enhancer in the same TAD. Thus, while previous studies have observed that allele-specific enhancers tend to be highly interconnected with other allele-specific enhancers (Prescott *et al*., 2015; Link *et al*., 2018), which has been interpreted to suggest that CREs within the same topological domain can modulate each other's function, our data indicate that locus-scale, *cis*-acting mechanisms exert limited effects on enhancer activity.

Next, we examined the extent to which *trans*-acting effects contribute to changes in *cis*-regulatory function and gene expression between each of the F_1-hybrid MEF lines. *Trans*-acting mechanisms should, in principle, affect each allele within the same F_1 hybrid equally, but genetic variation between the distinct F_1-hybrid MEF lines could confound quantitative comparisons of allele-specific enhancer function between each of the F_1 hybrids. To measure inter-F_1, *trans*-acting differences, we examined chromatin state and gene expression on the C57BL/6J X-chromosome, which is present across all F_1-hybrid lines. Applying the same criteria that we had used for defining allele-specific CREs on autosomes, we did not observe any CREs with significantly different H3K27ac levels on the C57BL/6J X-chromosome between F_1 hybrids (**Figure 2 – figure supplement 2A**). A similar analysis of chromatin-associated RNA-seq data revealed that expression of a small subset of C57BL/6J X-chromosome genes differed significantly between different F_1-hybrid strains. For example, 9.3% of expressed genes on the C57BL/6J X-chromosome differed by >2-fold in expression between C57BL/6J x

CAST/EiJ and C57BL/6J x SPRET/EiJ MEFs (**Figure 2 – figure supplement 2B**). This includes a number of genes critical for transcriptional regulation across the genome, such as *Smarca1,* which is expressed at ~2-fold lower levels in C57BL/6J x SPRET/EiJ hybrid MEFs compared to all other F_1-hybrid MEFs we surveyed). Taken together, these data suggest that *trans*-acting effects have a limited impact on histone modification levels at CREs and on gene transcription across these distinct F_1 hybrid strains. Therefore, for some subsequent analyses, we chose to merge chromatin and TF-binding data from allele pairs across different F_1-hybrid lines.

Distribution of genetic variants that influence *cis*-regulatory function

To characterize the types of variants that occur within CREs that cause changes in enhancer activity, we started by examining active enhancers with the largest differences in H3K27ac between alleles. We reasoned that these enhancers would contain large-effect, loss-of-function mutations on one allele, which could reveal TF-binding sites likely required for enhancer function. Across nine F1-hybrid strains, we identified a total of 29,185 pairs of enhancer alleles with a significant and >2-fold difference in H3K27ac levels between alleles. Allele-specific enhancers have a significantly higher frequency of SNPs/indels than H3K27ac signal-matched shared enhancers (**Figure 2C**). Moreover, enhancers with a greater number of genetic variants are more likely to show larger quantitative differences in H3K27ac levels (**Figure 2F-G**). Across many mammalian species, loci comprising allele-specific enhancers in F_1-hybrid MEFs exhibit slightly less evolutionary sequence conservation than those located at shared enhancers (**Figure 2 – figure supplement 1F**). On the other hand, active

promoters and gene-distal CTCF peaks tolerate, from a functional standpoint, a greater number of SNPs/indels than enhancers (**Figure 2D-E**).

We also hypothesized that the location of genetic variants within the enhancer is likely to impact whether a given SNP/indel affects enhancer function. To explore this further, we examined the distribution of SNPs/indels relative to the center of the accessible chromatin region at pairs of enhancer alleles with allele-specific or shared H3K27ac levels. This revealed an enrichment of SNPs/indels within a 150 bp window centered on the ATAC-seq summit at allele-specific enhancers (**Figure 2H**). In contrast, there was not a similar enrichment of SNPs/indels in allele-specific H3K4me3 peaks at promoters (**Figure 2J**). We also examined enhancer loci with a single SNP/indel present, since these sites can inform us about genetic variants that are sufficient to block enhancer function. We found that 14.6% of 1-SNP/indel enhancers show an allele-specific and >2-fold skew in H3K27ac levels, and we observed a more focal enrichment directly at the central region of the enhancer (which we define as the middle ~100 bp of the <200 bp accessible chromatin window) of SNPs/indels at allele-specific enhancers (**Figure 2I**). Together, these data suggest that the central region is most likely to harbor SNPs/indels that significantly modulate chromatin state at enhancers.

Identification of TF-binding motifs required for enhancer activity in MEFs

We next sought to determine candidate TF motifs that are required for enhancer activity in MEFs. Analysis of the top decile of active MEF enhancers (based on relative H3K27ac levels) in the C57BL/6J genome using the KMAC algorithm (Guo *et al*., 2018)

generated an output of several k-mers (i.e. nucleotide sequences of k length) that we manually matched to known binding motifs for several TF families (AP-1, TEAD, and ETS; **Figure 3 – figure supplement 1A**; **Supplementary File 6**). For AP-1, the k-mer identified by KMAC (5'-VTGACTCAB-3'; V indicates A/C/G and B indicates C/G/T) includes the known core AP-1 site (known as a TRE; TGASTCA; S indicates C/G), which is bound by heterodimers of Fos and Jun family TFs or homodimers of Jun family members (Risse *et al*., 1989; Eferl and Wagner, 2003). VTGACTCAB is the most enriched k-mer at active fibroblast enhancers (30.8%, versus 1.6% of control sequences; AUC = 0.450). AP-1 TFs bind DNA as dimers, with the basic leucine zipper (bZIP) DNA-binding domain of each Fos/Jun monomer recognizing half of a palindromic consensus motif. Because k-mer based motif representations make it possible to capture internucleotide dependencies (that are lost in position weight matrix (PWM) representations of TF-binding motifs), we were able to observe that certain flanking nucleotides on either side of the TRE are strongly depleted from bound AP-1 motifs relative to all occurrences genome-wide (i.e. T and A were depleted from the nucleotide on the 5' and 3' ends of the AP-1/TRE motif, respectively).

KMAC also identified an enriched k-mer (5'-GGAATK-3'; K indicates G/T) that matches the known core binding motif for the TEAD family of TFs (GGAAT; Farrance *et al*., 1992) and includes an additional restricted nucleotide on the 3' end (10.9%, versus 0.6% of control sequences; AUC = 0.289). TEAD TFs are broadly expressed in developing and adult cell types and function as transcriptional effectors of the

391 Hippo/YAP/TAZ signaling pathway that regulates cell growth and proliferation (Chen *et*
392 *al*., 2010).
393
394 We observed a similar enrichment of AP-1 and TEAD k-mers at both
395 constitutively active enhancers and enhancers that control transcription of late-response
396 genes activated by serum stimulation (identified in Vierbuchen *et al*., 2017; **Figure 3 –**
397 **figure supplement 1B**). This finding suggests that the specific dynamics of enhancer
398 activation cannot be readily distinguished by the presence or absence of these TF-
399 binding motifs alone, and suggests that the sequence features that determine whether
400 an enhancer is constitutively active or signal-responsive are more complex and remain
401 to be identified (Bevington *et al*., 2016; Comoglio *et al*., 2019).
402
403 Since these extended AP-1 and TEAD motifs were defined by their enrichment at
404 enhancers in the C57BL/6J genome (in comparison to GC-matched control regions), we
405 next sought to determine the impact of SNPs within these motifs on AP-1 and TEAD
406 binding at active enhancers using allele-specific TF-binding data (**Figure 3A-B**). We
407 performed a series of validations to ensure that distinct methods (ChIP-seq and
408 CUT&RUN) were providing similar quantitative information on TF-binding levels (**Figure**
409 **3 – figure supplement 2A-G**). We reasoned that an increased frequency of SNPs in
410 allele-specific enhancers would occur only at nucleotides required for sequence-
411 dependent binding of these TFs and not at neighboring regions flanking these
412 nucleotides (Maurano *et al*., 2015). For active enhancer loci with allele-specific Fos
413 binding, an enrichment of SNPs is observed at the core AP-1 motif (**Figure 3C**; n = 263

414 allele pairs). Within the core motif, the lowest enrichment of SNPs was observed at the
415 central nucleotide, consistent with *in vitro* experiments suggesting that this nucleotide
416 does not strongly influence AP-1-binding affinity (Risse *et al*., 1988). Recent *in vitro*
417 studies of AP-1 binding affinity to AP-1/TRE motifs suggests that the three nucleotides
418 flanking the core AP-1 motif (TGASTCA) can strongly modulate AP-1 TF binding by
419 altering the shape of the AP-1/TRE motif (Leonard and Kerppola, 1998; Rohs *et al*.,
420 2010; Yella *et al*., 2018). Given these data, we assessed whether these flanking
421 sequences play a role in determining AP-1 binding site selection in chromatin. Our data
422 in **Figure 3C** suggests SNPs at the 5' and 3' flanking nucleotides of the AP-1/TRE motif
423 (VTGACTCAB) can affect AP-1 binding at active Fos-bound enhancers. More broadly,
424 there is an enrichment of SNPs in the three nucleotides flanking each side of the core
425 AP-1 binding site when considering all allele-specific Fos-bound sites from our data
426 (NNVTGACTCABNN; 9.9% and 5.6% at allele-specific and shared Fos peaks,
427 respectively; **Figure 3 – figure supplement 1C**). These results provide further evidence
428 that sequences immediately flanking core AP-1 motifs should be considered in future
429 assessments of AP-1 binding motif preferences.
430
431 Next, we found that an additional nucleotide beyond the core TEAD-binding site
432 (GGAAT) was restricted to G/T in the KMAC output (GGAATK), and SNPs were
433 enriched at all positions within this motif at allele-specific Tead1-bound enhancers
434 (**Figure 3D**). For allele-specific CTCF sites with >2-fold difference in signal, we found a
435 ~14 bp window of enriched SNPs (i.e. broader than typical DNA-binding TFs, like AP-1
436 or TEAD) that disrupt CTCF binding (**Figure 3E**), closely mirroring the ~15-20 bp

sequence that CTCF is predicted to bind *in vivo* (Kim *et al*., 2007). These data indicate that AP-1 and TEAD motifs are the most enriched TF motifs within active enhancers in fibroblasts and functionally validate the importance of motif-flanking nucleotides for TF binding in the native chromatin context.

We next sought to use our allele-specific TF-binding data to perform a targeted analysis of how an allele-specific loss in AP-1 or TEAD occupancy impacts enhancer chromatin state. We separately identified a set of active enhancers that have a single instance of their core motifs (TGACTCA or GGAAT) and have a SNP/indel that alters this binding motif into a sequence not predicted to bind AP-1 or TEAD based on *in vitro* binding experiments, respectively. For both classes of TFs, motif-disrupting SNPs are correlated with a marked loss of binding of their cognate TFs, as expected, but this incomplete loss (in aggregate) also suggests that SNPs within core motifs alone are not completely predictive of changes in AP-1 or TEAD binding (**Figure 3F, 3J**). Loss of AP-1 binding is associated with a substantial decrease in chromatin accessibility, H3K4me1/2, and H3K27ac levels on the allele with the mutated AP-1 site (**Figure 3G-I**), consistent with our previous observations from a smaller set of enhancers (Vierbuchen *et al*., 2017). This finding suggests that at enhancers that contain a single consensus AP-1 site and are bound by Fos/Jun, a variant that changes a nucleotide in the core AP-1 motif is likely to result in a complete loss of enhancer function, consistent with data from a smaller set of plasmid-based reporters that suggest AP-1 motifs are required for transcriptional activation (Malik *et al*., 2014; Liu *et al*., 2016). Similar analysis of Tead1-bound enhancers revealed a more modest decrease in ATAC-seq, H3K4me1/2, and

H3K27ac signal associated with the allele lacking a predicted TEAD motif (**Figure 3K-M**), suggesting that loss in TEAD occupancy has less severe consequences on enhancer function than loss of AP-1 binding. Nevertheless, these data suggest that both AP-1 and TEAD motifs play a central role in enhancer function in fibroblasts.

AP-1 TFs facilitate binding of TEAD TFs to enhancers

Although SNPs that disrupt core TF-binding motifs (AP-1, TEAD, and ETS) are enriched at enhancers with allele-specific TF binding, our data also indicate that SNPs in these motifs are not sufficient to explain all instances of functional variation between enhancer alleles. For example, among all enhancers in the top decile of allele-specific H3K27ac signal, only 13.3% had a SNP/indel overlapping a core AP-1, TEAD, and/or ETS motif in their central region. In contrast, we found that 21.5% of allele-specific CTCF binding sites (with >2-fold difference in CTCF signal) that contain a CTCF motif (identified using position weight matrix match) had at least one SNP/indel overlapping the CTCF binding site. These data favor a model in which other types of SNPs outside core TF-binding motifs can collectively modulate enhancer activity.

In previous work, we found that strain-specific instances of AP-1 TF binding in MEFs (in a comparison of two inbred mouse strains) that lack a mutation in a core AP-1 site were enriched for SNPs in TEAD motifs, suggesting a model in which AP-1 binding was dependent, at least in part, on the presence of TEAD binding sites (Vierbuchen *et al*., 2017). However, we lacked TEAD binding data, which prevented us from examining in depth the sequence determinants and functional relationship of AP-1 and TEAD

binding at enhancers across the genome. Other data have suggested that AP-1 and TEAD TFs coordinately regulate transcriptional programs critical for cell growth and proliferation during normal development and in the context of cancer (Liu *et al*., 2016; Zanconato *et al*. 2018; Park *et al*., 2020; He *et al*., 2021). Since multiple AP-1 and TEAD TFs are also often co-expressed in the same cell types and can play functionally redundant roles with one another (Seo *et al*., 2021), it has been difficult to examine how these two TFs that exhibit extensive co-occupancy work together at enhancers to regulate gene transcription. With our newly generated AP-1 and TEAD binding data across four wild-derived inbred F_1-hybrid lines, we could more systematically examine a larger number of loci to define the functional relationship between AP-1 and TEAD.

We first quantified how often consensus TF motifs are mutated at allele-specific versus shared AP-1 and TEAD peaks. If the binding of a given TF was entirely dependent on the occupancy of another TF, we would expect to observe a similar loss in binding of the dependent TF, regardless of which TF motif was mutated. For these analyses, we included all distal Fos and Tead1 peaks in our dataset, including those that do not co-occur with H3K27ac. We observed that AP-1 motif mutations are frequently associated with a loss of TEAD binding, whereas AP-1 binding is more weakly affected by TEAD motif mutations (**Figure 4A-B**). Strikingly, AP-1 motif mutations were as enriched at allele-specific TEAD peaks as TEAD mutations were (compared to sites with shared TEAD binding). Analysis of AP-1 and TEAD co-bound sites (independent of whether they contained consensus AP-1 or TEAD motifs) further supported a hierarchical binding relationship between these TFs. For example, 50.2%

(n = 821/1,635 allele pairs) of allele-specific Fos-bound sites also exhibit an allele-specific loss of Tead1 binding, whereas only 8.7% (n = 821/9,416 allele pairs) of allele-specific Tead1 peaks showed significant allele-specific Fos signal. In summary, these data are consistent with previous studies that suggest that AP-1 can serve as a pioneer TF to facilitate the binding of other TFs, such as the glucocorticoid receptor, PU.1, and C/EBP (Biddie *et al*., 2011; Heinz *et al*., 2013), and that AP-1 binding is required for inducible chromatin remodeling and nucleosome displacement at late-response gene enhancers in fibroblasts (Vierbuchen *et al*., 2017).

Data from *in vitro* studies examining TF-binding specificity have shown that TFs that bind to composite motifs often prefer sequences that are distinct from their consensus individual motifs (Jolma *et al*., 2015). This led us to consider the possibility that sites at which AP-1 and TEAD bind together might exhibit differential motif requirements from sites where only one of these two TFs bind. We observed that AP-1-only peaks contain at least one AP-1 k-mer found using KMAC (65.9%; VTGACTCAB, VTGAATCAB, or VTTAGTCAY), whereas AP-1/TEAD co-bound peaks were less likely to contain a consensus motif (53.8%; **Figure 4C**). Similarly, TEAD-only peaks (44.0%) had a higher frequency of TEAD k-mers identified with KMAC (GGAATK) than AP-1/TEAD peaks (36.0%; **Figure 4D**). These data suggest that the motif requirements for AP-1/TEAD co-bound regions are slightly more flexible than sites at which only one of the TFs bind.

Identification of sequence features that determine AP-1/TEAD co-binding at enhancers

Thus far, our data suggest that many instances of AP-1 and TEAD binding cannot be explained solely by mutations in consensus, core motifs for these TFs. This lack of enriched TF motif mutations has been observed for other classes of TFs and in a variety of model systems, suggesting that this is a general, unresolved problem in genetic studies of TF binding (Deplancke *et al*., 2016). Our dataset allowed us to systematically look for recurrent features of SNPs/indels associated with allele-specific AP-1 or TEAD binding outside of core motifs for these TFs. These analyses can help reveal additional sequence motifs that influence AP-1 and TEAD binding, such as binding sites for other TFs that bind together with AP-1 or TEAD to establish chromatin accessibility. In particular, SNPs outside known TF-binding sites allow us to dissect the role of motif spacing on the ability of TFs to cooperate with one another to bind enhancers. Subtle changes in motif syntax have been shown to alter enhancer function (Erceg *et al*., 2014; Farley *et al*., 2016; Shen *et al*., 2021), and conversely, the arrangement of TF-binding motifs can also be highly flexible in other contexts (Arnosti and Kulkarni, 2005; Junion *et al*., 2012; King *et al*., 2020; Jindal and Farley, 2021).

First, we identified allele-specific gene-distal binding sites for Fos, Tead1, and CTCF, and then examined the frequency of SNPs/indels (relative to the ATAC-seq peak center) at these sites compared to sites with shared binding on both alleles. In **Figure 2I**, we plotted SNP/indel distributions at enhancers with allele-specific histone acetylation, whereas these analyses focus instead on TF-binding sites independent of

551 H3K27ac levels. When comparing allele-specific and shared TF peaks, we found an
552 increased frequency of SNPs/indels within an ~100 bp window centered on the ATAC-
553 seq peak summit, which is similar to the pattern observed at enhancer loci with allele-
554 specific H3K27ac levels (**Figure 5A-C**).
555
556 Next, given that AP-1 motif SNPs likely contribute to the distribution observed in
557 **Figure 5A**, we repeated this analysis, but excluded allele-specific AP-1 peaks that have
558 a SNP/indel in their extended AP-1 motif (VTGACTCAB) and plotted the SNP/indel
559 frequency relative to this motif instead of the ATAC-seq peak summit. This revealed an
560 enrichment of SNPs/indels within +/- ~50 bp of the AP-1 motif (**Figure 5D**). SNPs/indels
561 were similarly distributed relative to TEAD motifs at TEAD peaks (**Figure 5E**). These
562 observed patterns of SNPs/indels are consistent with a collaborative competition model
563 for AP-1 and TEAD binding. The collaborative competition model provides an
564 explanation for how TFs gain access to enhancer sequences that form nucleosomes. In
565 this model, simultaneous binding of multiple TFs is thought to be essential to
566 outcompete high-affinity interactions of histone octamers with these enhancer DNA
567 sequences. Biophysical experiments suggest that these collaborating TFs must bind to
568 the same half of the nucleosome to compete against the histone octamer for binding
569 (i.e. the same side relative to the nucleosome dyad, <75 bp from one another; Miller and
570 Widom, 2003; Moyle-Heyrman *et al*., 2011).
571
572 In contrast with the pattern of SNPs observed at allele-specific AP-1 and TEAD
573 peaks**,** when we plotted the distribution of SNPs/indels at allele-specific and shared

CTCF peaks, we observed a narrow enrichment of SNPs (within +/- ~10 bp) relative to the CTCF motif at allele-specific compared to shared peaks (**Figure 5F**). This result indicate a more restricted length scale at which genetic variants can disrupt CTCF binding than those that we observed for Fos and Tead1, and suggests that CTCF binding is less dependent on binding of additional, collaborating TFs.

Contribution of partial or degenerate AP-1 motifs to AP-1 binding affinity

Binding of TFs to their cognate motifs on nucleosomes is often restricted by steric hindrance between TFs and histone octamers. In particular, some pioneer TFs are thought to preferentially bind partial motifs over full motifs on nucleosomes (Soufi *et al*., 2015; Roberts *et al*., 2021). We considered the possibility that some instances of allele-specific AP-1 binding where there is an absence of a core AP-1 motif mutation could be explained by SNPs in nearby partial or degenerate TF-binding motifs not readily detected by traditional searches.

To examine whether binding to AP-1 half sites contributes to AP-1 recognition at enhancers, we chose to examine the frequency of TGASVDB k-mers at AP-1 bound sites. It should be noted that this motif is able to identify AP-1 half sites, and at the same time, capture degenerate or low-affinity AP-1 motifs that are difficult to detect from traditional motif searches because they bear little resemblance to predicted core motifs (Kribelbauer *et al*., 2019). Allele-specific and shared AP-1 peaks contained, on average, a similar number of AP-1 half sites (in the context of TGASVDB motifs; mean = 1.17 and 1.20 occurrences per peak in the central 150 bp, respectively). However, we observed a

~2-fold greater frequency of AP-1 half sites containing SNPs (TGASVDB) in allele-specific versus shared Fos peaks (mean = 0.25 and 0.13 occurrences per peak, respectively), suggesting that AP-1 half sites contribute to AP-1 TF binding in chromatin. However, based on our prior analysis of mutations in full AP-1 sites, it is clear that disruption of one of two half sites within an AP-1 consensus motif has a strong effect on AP-1 binding in most cases, which suggests that AP-1 half sites alone might not be sufficient for binding in the absence of another intact AP-1 motif at the same enhancer (**Figure 3C, 3F**). Thus, we favor a model in which AP-1 half sites play an accessory role in modulating levels of AP-1 occupancy, and are unlikely to be sufficient for AP-1 binding by themselves in the absence of a full AP-1 motif.

Identification of k-mers predictive of AP-1 binding and/or activity using machine learning

Since core TF-binding motifs alone cannot fully distinguish TF-bound alleles from those in which TFs are bound, we reasoned that additional k-mers could contribute to our ability to distinguish TF-bound sites versus non-bound sites in the C57BL/6J genome, and whether the identification of these k-mers might help identify other motifs that are recurrently mutated in our allele-specific TF-binding data. Therefore, we applied a gapped k-mer SVM approach (gkm-SVM) to our datasets that has been optimized to detect k-mers of similar length to typical TF-binding motifs (Ghandi *et al*., 2016). Support vector machine (SVM) algorithms have been utilized in a variety of contexts to perform classification of DNA sequences in a supervised manner (Barozzi *et al*., 2014; Ghandi *et al*., 2016; VandenBosch *et al*., 2022). It should be noted that k-mers identified

by gkm-SVM are simply DNA sequences of k length that can discriminate two sets of input sequences, and do not necessarily correspond to TF-binding sites per se.

We first compared 60 bp of DNA sequences from AP-1 peaks in C57BL/6J MEFs (positive set) to GC- and length-matched, randomly sampled background DNA sequences from the C57BL/6J genome (negative set). The area under the receiver operating characteristic curve (AUROC = 0.872) from this gkm-SVM analysis is highly similar to the corresponding value obtained from a control analysis of CTCF peaks from human cells, suggesting that the gkm-SVM is able to classify Fos-bound and unbound regions with a low rate of detecting false positives while correctly assigning true negatives. Similarly, a relatively high value for the area under the precision-recall curve (AUPRC = 0.881) indicates that the gkm-SVM is able to reliably distinguish true and false positives. Together, these results suggest that the information within the central 60 bp sequences (+/- 30 bp relative to the ATAC-seq summit) at Fos-bound peaks is sufficient to train a model to reliably distinguish Fos-bound sites from control non-coding regions of the same genome (**Figure 6 – figure supplement 1A**). Inclusion of additional sequence beyond this central 60 bp (up to a total of 300 bp) had only a slight positive effect on the performance of the model (**Figure 6A-B**). Conversely, shortening of DNA sequence below 60 bp resulted in a drop-off in performance of the model. k-mers containing AP-1 sites were the largest contributors to the performance of the model, as expected (**Figure 6 – figure supplement 1D**). Next, to determine whether sequences outside of the AP-1 motif contribute to the performance of the model, we repeated this same analysis, but we computationally masked all occurrences of core

643 AP-1 sites. This revealed a slight drop in AUROC (unmasked = 0.874, masked = 0.804)
644 and AUPRC (unmasked = 0.884, masked = 0.794) values, suggesting that the model
645 retains some predictive capacity when core AP-1 motif sequences are excluded (**Figure**
646 **6A-B, Figure 6 – figure supplement 1E**).
647
648 Interestingly, k-mers containing AP-1 sites also contributed the most to model
649 performance when gkm-SVM was applied to Tead1-bound sites (**Figure 6, figure**
650 **supplement 1B, 1F**), consistent with our observations that AP-1 binding is required for
651 TEAD binding at many enhancers (**Figure 5**). When we ran the gkm-SVM on CTCF
652 peaks, we observed a highly distinct set of enriched k-mers from those found at AP-1
653 peaks. Many of these identified k-mers matched the well-documented CTCF binding
654 site, as expected (**Figure 6 – figure supplement 1C, 1G**).
655
656 We next sought to apply this gkm-SVM approach to attempt to identify k-mers
657 that distinguish between AP-1 binding sites with and without H3K27ac. Our data
658 indicate that the AP-1 binding is required for the function of many of the active
659 enhancers at which they bind in MEFs. However, AP-1 binding alone is clearly not
660 sufficient for enhancer activity. For example, 34.9% of gene-distal Fos peaks do not
661 overlap H3K27ac peaks. This suggests that the sequence features that are permissive
662 for AP-1 binding in MEFs might be separable from those that confer activity. For this
663 gkm-SVM analysis, we selected a curated set of Fos-bound allele pairs (n = 2,697) that
664 (1) have equivalent levels of Fos binding, (2) contain a consensus AP-1 site on both
665 alleles, but (3) exhibit allele-specific H3K27ac levels. We input 60 bp DNA sequences

(centered on the shared AP-1 consensus motif) from the active (positive set) and inactive (negative set) alleles at Fos-bound enhancers (**Figure 6 – figure supplement 1H**). In contrast to the results above, the gkm-SVM failed to discriminate between these two sets of sites (AUROC = 0.086 and AUPRC = 0.318), suggesting that sequence features predictive of H3K27ac are more complex and cannot be readily captured by this k-mer based SVM approach.

Generalizability of sequence determinants of AP-1 binding across cell types and species

Having defined some features of sequences that determine AP-1 binding to CREs in MEFs, we next extend our analyses to data derived from a larger number of other cell types. To do this, we used DNase-seq footprinting data generated from a large panel of human tissues and cell types (Vierstra *et al*., 2020). These data provide an unbiased view of individual TF-DNA binding interactions within CREs.

First, we identified TF footprints that overlap an extended AP-1 motif (VTGACTCAB) within CREs, which we interpret as individual instances of AP-1 binding. We found a total of 164,705 TF footprints (from among >4 x 10^6 total footprinted regions) that contain VTGACTCAB motifs. These AP-1 footprints were centrally enriched within CREs (**Figure 6C**,) consistent with the distribution of AP-1 k-mers observed at AP-1 bound peaks in MEFs, as well as previous data examining AP-1 motif frequency within human DNase-seq peaks (Grossman *et al*., 2017). The majority of AP-1 footprints were <30 bp in width (83.3%; median = 17 bp), which suggests that they

represent the footprint caused by binding of a single AP-1 homo/heterodimer (**Figure 6D**. CREs with AP-1 footprints typically have a total of ~3-4 additional TF footprints (**Figure 6E**), and the median distance between AP-1 footprints and the nearest other TF footprint is ~24 bp (**Figure 6F**). gkm-SVM analysis of sequences flanking AP-1 footprints (60 bp windows) revealed an enrichment of TEAD and ETS k-mers, consistent with our observations at AP-1 bound sites in MEFs (**Figure 6 – figure supplement 1I**). Together, these data suggest a model in which AP-1 is critical for CRE function across many cell types and provide further insight into the nature of TF-binding events that occur with AP-1 binding at CREs active across cellular contexts, such as TEAD and ETS. These data will be valuable for disentangling the complex sequence features that control AP-1 binding and enhancer function across diverse cell types and tissues.

DISCUSSION

In this study, we leverage natural genetic variation across inbred mouse strains to identify sequence variants associated with differential TF binding and/or enhancer activity in their endogenous genomic context. To systematically assess the effect of many genetic variants on CRE function, we mapped TF binding (AP-1, TEAD, CTCF) and multiple chromatin features (ATAC-seq, H3K27ac, H3K4me1/2, H3K4me3) in up to ten distinct alleles for each CRE locus. By assessing the frequency and distribution of genetic variants at large numbers of CREs with shared or allele-specific TF binding and/or *cis*-regulatory activity, we define features of *cis*-acting genetic variants that are most predictive of differences in chromatin state and/or TF binding.

We find from our analysis of enhancer alleles with different H3K27ac levels that loss of the active enhancer histone modification H3K27ac is generally not genetically separable from loss of H3K4me1/2. This is interesting to consider given a number of previous observations about the relative contribution of these histone modifications to enhancer function: (1) we previously found that enhancers that regulate late-response genes exhibit H3K4me1 enrichment in serum-starved MEFs, but have low chromatin accessibility and lack H3K27ac, and upon serum-stimulation, gain H3K27 acetylation and inducibly bind AP-1 TFs (Vierbuchen *et al*., 2017), (2) recent studies suggest that enhancers with H3K4me1 enrichment that lack H3K27ac are not, in fact, poised for future activity, but instead that this chromatin state is a remnant of activity in a recent, prior developmental stage (Kim and Shiekhattar, 2015; Jadhav *et al*., 2019), and (3) catalytic mutants of Mll3/4, enzymes responsible for H3K4me1/2 deposition, do not appear to affect recruitment of RNA polymerase II to enhancers suggesting that the H3K4me1/2 modification is not required for enhancer function (Dorighi *et al*., 2017; Jang *et al*., 2017; Rickels *et al*., 2017). Taken together, these observations suggest that in a given cell type or context, H3K4me1/2-only enhancers might exhibit different *cis*-regulatory features compared to enhancers that have H3K27ac enrichment because they represent enhancers that were active in a previous developmental stage characterized by a distinct complement of TFs expressed.

The functional sequence variants between inbred mouse strains that we identified provide insight into enhancer turnover that occurs across evolution (Villar *et*

735 *al*., 2015). We find that greater numbers of SNPs/indels at enhancers are correlated
736 with higher probabilities of allele-specific enhancer activity, and that allele-specific
737 enhancers in fibroblasts are also less conserved across species than shared
738 enhancers. Enhancers are thought to turn over rapidly because many loci contain
739 multiple enhancers with overlapping *cis*-regulatory activity, such that loss of any
740 individual single enhancer is often insufficient to cause a large change in gene
741 expression and/or result in an organismal phenotype (Osterwalder *et al*., 2018). It would
742 also be interesting to examine how the impact of SNPs on enhancer activity correlates
743 with their frequency in natural populations or whether the SNP represents a derived or
744 ancestral state across the broader rodent lineage, as SNPs with larger impacts on
745 enhancer function would be expected to be found at lower frequencies if they are
746 potentially deleterious to overall fitness.
747
748 We also found that SNPs/indels that are associated with allele-specific H3K27ac
749 levels tend to occur within ~50 bp of the center of the accessible chromatin region used
750 to define enhancer sequences. This is further supported by enhancer loci in which
751 alleles differ by a single SNP/indel. At such enhancer alleles, these single sequence
752 variants are almost certainly causal and thus likely to explain observed differences in
753 enhancer activity. Together, these data suggest that SNPs within the central region of
754 enhancers should be prioritized in genome-wide association studies for human traits
755 and/or disease risk.
756

757 The distribution of SNPs that impact AP-1 binding to enhancers is interesting to
758 consider in the context of a recent paper that looked at sequence features that
759 distinguish AP-1 bound enhancers with high versus low activity in reporter assays
760 (Chaudhari and Cohen, 2018). Their analysis using a supervised machine learning
761 approach (gkm-SVM) suggests that most of the variation in AP-1 bound enhancer
762 activity can be predicted using input sequences that consist of the AP-1 core motif and
763 an additional +/- 10 bp on each side. The close proximity of these sequences to AP-1
764 sites contrasts with the broader window (+/- ~50 bp relative to AP-1 motifs) that we
765 observe to be important for determining AP-1 binding to chromatin in fibroblasts. More
766 generally, these observations suggest that the sequence determinants of enhancer
767 activity might be more complex within the genomic context than what has been
768 observed in reporter assays. In addition, we found that the gkm-SVM has limited ability
769 to predict activity levels of AP-1 bound sites, suggesting that deep learning approaches
770 might be required to delineate higher-order sequence features associated with active
771 enhancers in a given cellular context (Avsec *et al*., 2021; de Almeida *et al*., 2022).
772
773 The observed requirement for AP-1 for TEAD binding to enhancers is interesting
774 to consider given that these two distinct TFs have been previously shown to co-regulate
775 gene expression programs associated with cell proliferation and tissue growth. Both AP-
776 1 and TEAD are transcriptional effectors of intercellular signaling pathways. AP-1 TFs
777 are activated by Ras/MAPK signaling and TEAD TFs are required for the binding of the
778 transcriptional co-activators YAP and TAZ, whose nuclear localization is directly
779 regulated by Hippo signaling. Our data suggests a mechanism for crosstalk between

these two signaling pathways in which the transcriptional output of the Hippo pathway can be modulated depending on whether Ras/MAPK is active or not. This instructive function of AP-1 in selecting the enhancers at which TEAD TFs can bind is similar to the role for AP-1 in facilitating the binding of transcriptional effectors from several other signaling pathways, including the glucocorticoid receptor, NF-κB, and SMAD (Biddie *et al*., 2011; Heinz *et al*., 2013; Li *et al*., 2019).

Enhancer sequences tend to be occluded by histone octamers prior to TF binding, suggesting that during the process of enhancer selection some TFs must be able to bind to their cognate motifs in a nucleosomal context (Tillo *et al*., 2010; Barozzi *et al*., 2014). This complicates efforts to determine sequence features required for TF binding because the affinity of a TF for nucleosomal and naked DNA often differ significantly. Furthermore, different classes of TFs utilize distinct mechanisms to engage with their cognate motifs on nucleosomes (Michael and Thoma, 2021). Based on *in vitro* nucleosome-binding studies, bZIP TFs, which include AP-1 TFs, can only bind to their cognate motifs on nucleosomes when their motifs are present on outer regions of nucleosomes (i.e. furthest from predicted dyad locations; He *et al*., 2013). These outer regions are thought to be more accessible for TF binding because they are intermittently unwound from the histone octamer (known as nucleosome breathing; Zhu et al., 2018; Zhou *et al*., 2019). This is consistent with structural data suggesting that AP-1 TFs cannot bind their full cognate motif (TGASTCA) on nucleosomes due to steric constraints (Michael and Thoma, 2021). We observe an enrichment of SNPs in AP-1 half sites (TGASVDB) at allele-specific AP-1 peaks, raising the possibility that partial

AP-1 motifs contribute to AP-1 binding to nucleosomal enhancers. The binding to partial motifs has been observed for other nucleosome-binding TFs, such as OCT4 (Soufi *et al*., 2015). Thus, we favor a model in which (1) AP-1 recognizes full motifs towards the edges of nucleosomes, (2) AP-1 dimers can then bind both halves of the core AP-1 site when it is accessible upon nucleosome breathing, (3) the initial binding of AP-1 facilitates the binding of other dependent TFs (e.g. TEAD) via collaborative competition to evict the histone octamer and/or recruit co-regulatory proteins and chromatin remodelers to enhancers, and (4) AP-1 might be able to bind half motifs absent nucleosome breathing at any position on the nucleosome. In future, fully delineating sequence requirements for AP-1 binding will require detailed *in vitro* and structural experiments using naturally occurring enhancer sequences, as well as deep learning approaches applied to genomic data of AP-1 binding from multiple cell types and genotypes (Avsec *et al*., 2021).

Our F_1-hybrid dataset has provided new insights into how DNA sequences within CREs contribute to TF binding and enhancer function. We believe that this F_1-hybrid approach for examining TF function is a powerful tool to uncover sequence determinants of TF binding that cannot be easily detected from PWM-based motif searches or motif enrichment analysis alone. Our F_1-hybrid datasets identify thousands of enhancer allele pairs that differ subtly in their DNA sequences and yet have strongly allele-specific functional properties. In the future, incorporating F_1-hybrid data from additional cell types can further reveal both context-specific and broadly applicable mechanisms of TF binding and enhancer activity (Halow *et al*., 2021). More broadly, this

F_1-hybrid approach represents a powerful tool for understanding complex *cis*-regulatory processes and can accelerate efforts to identify functional non-coding variants that contribute to human disease and complex traits.

MATERIALS AND METHODS

Mice

All animal experiments were approved by the National Institutes of Health and the Harvard Medical School Institutional Animal Care and Use Committee and were conducted in compliance with the relevant ethical regulations. 6-week-old female C57BL/6J mice were obtained from Jackson Labs (Bar Harbor, ME, USA) (Stock No. 000664) for all breeding pairs. 4- to 8-week-old male mice from the following strains were also obtained from Jackson Labs: CAST/EiJ (Stock No. 000928), MOLF/EiJ (Stock No. 000550), PWK/PhJ (Stock No. 003715), SPRET/EiJ (Stock No. 001146), 129S1/SvImJ (Stock No. 002448), A/J (Stock No. 000646), BALB/cJ (Stock No. 000651), DBA/2J (Stock No. 000671), NOD/ShiLtJ (Stock No. 001976). No new mouse strains were generated in this study.

The study of inbred mice that are more genetically divergent from C57BL/6J in combination with the use of longer sequencing reads increases the proportion of informative allele-specific reads. However, higher frequencies of SNPs/indels per strain results in a greater percentage of CREs with multiple genetic variants, making it difficult to assign which specific SNP/indel is likely responsible for observed changes in TF

binding or chromatin state. Therefore, to balance these considerations, we included wild-derived inbred strains with a relatively high frequency of SNPs/indels compared to C57BL/6J mice (1 SNP/indel per ~85-170 bp), as well as more commonly used inbred strains that are less genetically divergent from C57BL/6J mice (1 SNP/indel per ~1,000 bp; **Supplementary File 1**).

Generation of MEF lines

Embryos were harvested on embryonic day 13.5-14.5 and washed in room-temperature PBS. The heads and internal organs were removed, and the dissected tissue was re-washed in PBS. Individual embryos were placed at the center of 15-cm plates and incubated for 45 min in 1 mL trypsin-EDTA 0.25% (Life Technologies 25200072). Excess trypsin was carefully aspirated, and the dissected tissue was manually dissociated with scissors for ~1 min. Dissociated cells were then incubated in ~1 mL trypsin-EDTA at 37^{o}C in 5% CO_2 for 30 min. Complete media was prepared by supplementing DMEM (Life Technologies (Carlsbad, CA, USA) 12430062) with 10% CCS (Thermo Fisher (Waltham, MA, USA) SH3008704), Penicillin-Streptomycin (Thermo Fisher 15140148), MEM non-essential amino acids (Thermo Fisher 11140050), and 1 mM sodium pyruvate (Thermo Fisher 11360070). Trypsin was quenched with 10 mL complete media, and cells were rapidly triturated up/down 10 times with a 10 mL serological pipette to generate a single-cell suspension. An additional 10 mL complete media was added per plate, and cells were grown at 37^{o}C in 5% CO_2.

When cells became fully confluent in ~2-3 days, MEFs were washed in PBS and trypsinized in 3 mL trypsin-EDTA. A small aliquot of cells from each embryo were frozen for genotyping (see below). Cells were pelleted by spinning at 300 g and expanded onto five 15-cm plates with 20 mL complete media per plate. When fully confluent once again, MEFs were trypsinized and frozen down in freeze media (50% complete media, 40% CCS, and 10% DMSO) in aliquots of 1 plate per cryogenic vial. Cells were placed at -80^{o}C for ~24 hr in a cell freezing container and then transferred to liquid N_2 for long-term storage.

For genotyping, cells were processed with the DNeasy Blood and Tissue kit (QIAGEN (Hilden, Germany) 69506). All MEF lines were tested for mycoplasm contamination with the following primer pairs: 5'-CTTCWTCGACTTYCAGACCCAAGGCAT-3' (Myco2(cb)) with 5'-ACACCATGGGAGYTGGTAAT-3' (Myco11(cb)) and 5'-GGTGTGGGTGAGTTATTACAAARTCAATT-3' (Myco5(cb)) with 5'-GGAGTGAGTGGATCCATAAATTGTGA-3' (Myco6(cb)). Genotyping for the sex of each MEF line was performed with the following primer pair: 5'-CTGAAGCTTTTGGCTTTGAG-3' with 5'-CCACTGCCAAATTCTTTG-3'. A single 340 bp product was expected for female cells, and an additional 310 bp product was present in male cells.

Generation of Fos antibody

We generated an in-house antibody against the full-length mouse protein for c-Fos (NCBI Reference Sequence: NP_034364.1). Briefly, we purified GST-c-Fos-His as

detailed in Sharma *et al*., 2019 and injected the recombinant protein into immunocompromised rabbits. Serum was collected and affinity purified using a protein A column before use in ChIP-seq and CUT&RUN experiments.

Cell culture

Cells were thawed onto one 15-cm plate per MEF line and grown in complete media until fully confluent. For ChIP-seq and Hi-ChIP experiments, MEFs were split onto five 15-cm plates and grown in complete media until ~70-80% confluent. Cells were washed in 10 mL room-temperature PBS and switched into 20 mL warmed starve media (0.5% CCS, with the same supplement concentrations as complete media). After 26+ hours in starve media, samples to be serum stimulated were incubated with 20 mL warmed stimulation media (30% CCS, with the same supplement concentrations as complete media) for 0, 10, or 90 min.

For ATAC-seq, RNA-seq, and CUT&RUN experiments, MEFs were thawed as above and were split into 6-well dishes at a concentration of 5×10^5 cells per well in 2 mL warmed starve media. Cells were grown for 26+ hours, and appropriate wells were serum stimulated with 2 mL warmed stimulation media.

Crosslinking cells

Media was aspirated from MEFs, and 2 mL or 15 mL crosslinking buffer (10 mM HEPES pH 7.5, 100 mM NaCl, 1 mM EDTA, 1 mM EGTA) with 1% formaldehyde was added for 6-well or 15 cm dishes, respectively. Cells were crosslinked by shaking gently for 10

min at room temperature. Crosslinking was quenched by adding glycine to a final concentration of 125mM and incubating for 5 min at room temperature while shaking. Cells were washed once in 2 mL or 15 mL PBS for 6-well or 15 cm dishes, respectively. Cells were scraped and collected in 1 mL or 5 mL cold PBS for 6-well or 15 cm dishes, respectively, and pelleted by spinning at 1,000 g for 5 min at 4^{o}C.

ATAC-seq libraries

MEFs from a 6-well dish were washed twice in 1 mL cold PBS and pelleted each time by spinning at 300 g for 5 min at 4^{o}C. 50,000 MEFs were resuspended in 50 µL cold ATAC lysis buffer (10 mM Tris-HCl pH 7.5, 10 mM NaCl, 3 mM $MgCl_2$, 0.1% NP-40 0.1% Tween 20, 0.01% digitonin) and incubated for 3 min on ice. Lysed cells were washed once in 1 mL ATAC wash buffer (10 mM Tris-HCl pH 7.5, 10 mM NaCl, 3 mM $MgCl_2$, 0.1% Tween 20) by gently inverting the tube 3 times and pelleted by spinning at 500 g for 10 min at 4^{o}C. Pelleted nuclei were resuspended in 50 µL transposition mix (25 µL 2x TD Buffer (Illumina (San Diego, CA, USA) 20034197), 2.5 µL TDE1 transposase (Illumina 20034197), 0.5 µL 10% Tween 20, 0.5% 1% digitonin, 16.5 µL PBS, 5 µL NF-H_2O) and incubated for 30 min at 37^{o}C with a Thermomixer set to 1,000 rpm. Samples were purified with MinElute PCR Purification Kit (QIAGEN 28004) per manufacturer's instructions and eluted in 13 µL NF-H2O. Libraries were amplified by adding the following to 10 µL purified DNA: 2.5 µL 25 µM Ad1 universal primer, 2.5 µL 25 µM Ad2.* indexing primer, 25 µL NEBNext Hi-Fi 2x PCR Master Mix (NEB (Ipswich, MA, USA) M0541S), 10 µL NF-H_2O. After an initial 5 PCR cycles, libraries were quantified by qPCR by adding the following to 5 µL partially amplified DNA: 0.5 µL 25

uM Ad1 universal primer, 0.5 µL 25 µM Ad2.* indexing primer, 5 µL NEBNext Hi-Fi 2x PCR Master Mix, 0.15 µL 1x SYBR Green I (Thermo Fisher S7563), 3.85 µL NF-H_2O. All primer sequences referenced are described in Buenrostro *et al*., 2015. The number of additional PCR cycles required for amplifying remaining libraries was determined by the number of qPCR cycles needed to reach 1/3 of the maximum SYBR green signal. Libraries were purified with AMPure XP beads (0.5x volume; Beckman Coulter (Indianapolis, IN, USA) A63881), and the supernatant was retained to remove large fragments. Primer dimers were removed by a subsequent cleanup with AMPure XP beads (1.3x initial volume), and libraries were eluted in 20 µL NF-H2O. Libraries were sequenced on an Illumina NextSeq 500 with 40 bp paired-end reads.

ChIP-seq libraries

Crosslinked MEFs per protocol above from 15 cm dishes were resuspended in 1 mL L1 buffer (50 mM HEPES pH 7.5, 140 mM NaCl, 1 mM EDTA, 1 mM EGTA, 0.25% Triton X-100, 0.5% NP-40, 10% glycerol, 10 mM sodium butyrate) per 15 cm dish starting material and rotated for 10 min at 4^{o}C to lyse cells. Nuclei were pelleted by spinning at 1,350 g for 5 min at 4^{o}C and resuspended in 1 mL L2 buffer (10 mM Tris-HCl pH 8.0, 200 mM NaCl, 10 mM sodium butyrate) per 15 cm dish starting material and rotated for 10 min at room temperature. Nuclei were pelleted by spinning at 1,350 g for 5 min at 4^{o}C and resuspended in 300 µL LB3 buffer (10 mM Tris-HCl pH 8.0, 100 mM NaCl, 1 mM EDTA, 0.5 mM EGTA, 0.1% sodium deoxycholate, 0.5% N-lauroylsarcosine, 10 mM sodium butyrate) per 15 cm dish starting material. Chromatin was sonicated with a Bioruptor Plus (Diagenode (Denville, NJ, USA)) on “high” power setting with an “on”

964 interval of 30 sec and “off” interval of 45 sec for 36 cycles). DNA concentration was
965 determined by taking 100 µL aliquot of sonicated chromatin, decrosslinking at 95^{o}C for
966 15 min, and purifying with QIAquick PCR Purification Kit (QIAGEN 28104) and
967 quantifying by Nanodrop. 1 µg of purified chromatin in 10% glycerol was run on a 2%
968 agarose gel and stained with ethidium bromide for 30 min to validate fragment size
969 (typically within ~200-1,000 bp). The remainder of the sonicated chromatin was
970 transferred to 1.5 mL tubes and centrifuged at 16,000 g for 10 min at 4^{o}C to pellet
971 insoluble debris. Triton X-100 was added to soluble chromatin to a final 1%
972 concentration. Protein A Dynabeads (Thermo Fisher 10008D) were washed twice in 1
973 mL cold block solution (0.5% BSA (w/v), 1% Triton X-100, diluted in LB3 buffer). For
974 coupling antibodies to beads, 15 µL bead slurry per IP were resuspended in 1.5 mL cold
975 block solution, and the appropriate amount of antibody (0.5 ug for anti-H3K27ac (Abcam
976 (Waltham, MA, USA) ab4729), 0.5 µg for anti-H3K4me1 (Abcam ab8895), 0.5 µg for
977 anti-H3K4me2 (Abcam ab7766), 0.5µg for anti-H3K4me3 (Abcam ab8580), 2 µg for
978 anti-Fos (in-house generated antibody and Santa Cruz Biotechnology (Dallas, TX, USA)
979 sc-7202X), 2 µg for anti-Tead1 (Abcam ab133533), 2 µg for anti-CTCF (Active Motif
980 (Carlsbad, CA, USA) 61312), and 2 ug for anti-JunD (Santa Cruz Biotechnology sc74))
981 was added before rotating beads for >2 hrs at 4^{o}C. For pre-clearing chromatin, 15 µL
982 bead slurry was added to appropriate amount of chromatin (40 µg for histone
983 modifications, 80 µg for transcription factors), and additional cold LB3 buffer with 1%
984 Triton X-100 was added such that all samples had a final volume of 1.5 mL before
985 rotating samples for > 2 hrs at 4^{o}C. Pre-cleared chromatin was added to antibody-
986 coupled beads, and additional cold LB3 buffer with 1% Triton X-100 was added such

that all samples had a final volume of 1.8 mL before rotating samples overnight at 4°C. 50 µL of pre-cleared chromatin was stored at -20°C for making input libraries. For all wash steps listed below, samples were rinsed with 1 mL cold wash buffer and rotated for 5 min at 4°C before separating beads with a magnet and discarding supernatant. Samples were washed sequentially twice in low salt buffer (0.1% SDS, 1% Triton X-100, 2 mM EDTA, 20 mM Tris-HCl pH 8.0, 150 mM NaCl), twice in high salt buffer (0.1% SDS, 1% Triton X-100, 2 mM EDTA, 20 mM Tris-HCl pH 8.0, 500 mM NaCl), twice in LiCl buffer (250 mM LiCl, 1% NP-40, 0.5% sodium deoxycholate, 1 mM EDTA, 10 mM Tris-HCl pH 8.0), and once in TE buffer (50 mM Tris-HCl pH 8.0, 10 mM EDTA). Samples were eluted from beads by addition of 200 µL TE buffer with 1% SDS and incubating at 65°C for 30 min, with brief vortexing every 10 min to mix. IP samples were placed on magnet, and supernatant was transferred to new tubes. Input samples were also thawed, and 150 µL TE buffer with 1% SDS was added. Both IP and input samples were decrosslinked by incubating at 65°C overnight. 10 µg RNase A (Sigma Aldrich (St. Louis, MO, USA) R6513) was added and samples were incubated at 37°C for 1 hr to digest RNA. 7 µL 20 µg/µL proteinase K (New England Biolabs P8107) was added, and samples were incubated at 55°C for 2 hr to digest protein. DNA was extracted with 1 volume of 25:24:1 phenol-chloroform-isoamyl alcohol and purified with QIAquick PCR Purification Kit (QIAGEN 28104). Libraries were prepared with the Ovation Ultralow V2 DNA-Seq Library Preparation Kit (NuGEN (Redwood City, CA, USA) 0344NB-32) per manufacturer's instructions. Libraries were sequenced on an Illumina NextSeq 500 with 150 bp paired-end reads.

CUT&RUN libraries

Crosslinked MEFs per protocol above from 6-well dish were washed once in 2 mL PBS and collected in 1 mL cold NE1 buffer (20 mM HEPES pH 7.5, 10 mM KCl, 1 mM $MgCl_2$, 1 mM DTT, 0.1% Triton X-100, Roche Protease Inhibitor Cocktail (Millipore (Burlington, MA, USA) 11873580001)). Cells were permeabilized to isolate nuclei by rotating for 10 min at 4°C. Nuclei were pelleted by spinning at 500 g for 5 min at 4°C and resuspended in 1 mL cold CUT&RUN wash buffer (20 mM HEPES pH 7.5, 0.2% Tween-20, 150 mM NaCl, 0.1% BSA, 0.5 mM spermidine, 10 mM sodium butyrate, Roche Protease Inhibitor Cocktail). 10 µL concanavalin-coated bead slurry (Bangs Laboratories (Fishers, IN, USA) BP531) per sample was washed twice in 1.5 mL CUT&RUN binding buffer (20 mM HEPES pH 7.5, 10 mM KCl, 1 mM $CaCl_2$, 20 mM $MnCl_2$) and resuspended in a final volume of 10 µL CUT&RUN binding buffer per sample. After adding 10 µL bead slurry to each sample, tubes were inverted 10 times and incubated for 10 min at room temperature to bind nuclei. Beads were separated from wash buffer by placing on magnet for >30 sec and were resuspended in 50 µL antibody buffer (0.1% Triton X-100, 2 mM EDTA, diluted in CUT&RUN wash buffer). Antibodies (in-house anti-Fos, anti-H3K27ac (Abcam ab4927), or rabbit IgG (Cell Signaling Technology (Danvers, MA, USA) 2729S)) were added at 1:50 dilution, and samples were incubated overnight at 4°C. Beads were washed once in 1 mL Triton-wash buffer (0.1% Triton X-100, diluted in CUT&RUN wash buffer) and resuspended in 50 µL antibody buffer. Protein-A MNase (Skene and Henikoff, 2017) was added to a final concentration of 700 ng/mL, and samples were incubated for 1 hr at 4°C. Beads were washed twice in 1 mL Triton-wash buffer and resuspended in 100 µL Triton-wash buffer. 2 µL 100 mM $CaCl_2$ was added

per sample to activate the MNase and each sample incubated on ice for 30 min. 100 µL 2x STOP buffer (340 mM NaCl, 20 mM EDTA, 4 mM EGTA, 0.1% Triton X-100, 50 µg/mL RNase A (Sigma Aldrich R6513), 2 pg/mL yeast spike-in DNA (provided by S. Henikoff)) was added, and samples were incubated for 20 min at 37°C to release CUT&RUN fragments from nuclei. Samples were placed on magnet, and supernatant was transferred to a new tube and added to 2 µL 10% SDS and 2 µL 20 mg/mL proteinase K (New England Biolabs P8107). Samples were incubated overnight at 65°C to reverse crosslinks. DNA was extracted with 1 volume of 25:24:1 phenol-chloroform-isoamyl alcohol and precipitated in 2.5 volumes of 100% ethanol with 2 µL glycogen (Sigma Aldrich 10901393001). Pellet was washed once in 1 mL 100% ethanol and dissolved in 40 µL 10 mM Tris-HCl pH 8.5. Libraries were prepared as described in (Skene and Henikoff, 2017), with two subsequent AMPure XP bead cleanups (1.1x volume) to fully remove contaminating adapter dimers from libraries. Libraries were sequenced on an Illumina NextSeq 500 with 40 bp paired-end reads.

Hi-ChIP libraries

Hi-ChIP was performed as previously described in (Mumbach *et al*., 2017) with the following modifications. 15 µL of MboI restriction enzyme (New England Biolabs R0147) was used for digesting chromatin from 15 million MEFs. Sonication was performed with a Covaris M220 with the following settings: duty cycle = 5, PIP = 70, cycles/burst = 200, and time = 8 min. 75 µL of Protein A Dynabeads (Thermo Fisher 10008D) was used for IP and 1 µg of anti-H3K27ac (Abcam ab4927) antibody was used per sample to typically

yield 12.5 ng DNA. Accordingly, 0.6725 µL of transposase enzyme (Nextera 20034197) was used to insert adapters, and libraries were amplified for 8 PCR cycles.

RNA-seq libraries

MEFs from 15 cm dish were washed once in 15 mL cold PBS and pelleted by spinning at 300 g for 5 min at 4°C. Cell pellet was resuspended in 200 µL cold cytoplasmic lysis buffer (10 mM Tris-HCl pH 7.5, 150 mM NaCl, 0.15% NP-40) and rotated for 5 min at 4°C. Lysate was layered on top of 500 µL cold sucrose buffer (10 mM Tris-HCl pH 7.5, 150 mM NaCl, 24% sucrose (w/v)) and centrifuged at 16,000 g for 10 min at 4°C. These steps were repeated once more to achieve higher purity in the nucleoplasmic fraction. Pelleted nuclei were resuspended in 200 µL glycerol buffer (20 mM Tris-HCl pH 7.9, 75 mM NaCl, 0.5 mM EDTA, 50% glycerol, 0.85 mM DTT), and an equal volume of cold nuclear lysis buffer was added (20 mM HEPES pH 7.5, 7.5 mM $MgCl_2$, 0.2 mM EDTA, 300 mM NaCl, 1 M urea, 1% NP-40, 1 mM DTT). Tubes were gently vortexed twice for 2 sec, incubated for 1 min on ice, and centrifuged at 18,000 g for 2 min at 4°C. These steps were repeated once more to achieve higher purity in the chromatin fraction. The remaining chromatin pellet was resuspended in 50 µL cold PBS and vortexed briefly. 500 µL of TRIzol (Thermo Fisher 15596026) was added to the pellet and vortexed for several minutes until fully resuspended. Chromatin-associated RNA was isolated with RNeasy Mini Kit (QIAGEN 74104) per manufacturer's instructions, and libraries were generated from 250 ng starting material with NEBNext Ultra Directional RNA Library Prep Kit for Illumina (New England Biolabs E7765). Libraries were sequenced on an Illumina NextSeq 500 with 150 bp paired-end reads.

Pseudogenome generation

SNPs occurring in the CAST/EiJ, MOLF/EiJ, PWK/PhJ, and SPRET/EiJ genomes relative to the mm10 reference genome were obtained from SNP release version 5 of the Mouse Genomes Project (Keane *et al*., 2011). Only high-confidence SNPs annotated with the PASS filter, filtered using VCFtools (version 0.1.12; Danecek *et al*., 2011), were used in all analyses. A separate pseudogenome for each wild-derived inbred strain was constructed from these SNPs using Modtools (version 1.0.2; Huang *et al*., 2014).

Allele-specific read mapping

Reads were trimmed with the paired-end option and with SLIDINGWINDOW:5:30 using Trimmomatic (Bolger *et al*., 2014). Paired-end reads that survived trimming were re-paired using the bbmap utility (Bushnell 2014). Both unpaired and paired reads were concurrently mapped to the C57BL/6J and appropriate pseudogenome with bowtie2 using default parameters (Langmead and Salzberg, 2012). Mapped reads were converted to .bam format with samtools view (Li *et al*., 2009) using the following options -h -b -F 3844 -q 10 and sorted by coordinate. Reads initially mapped to each pseudogenome were converted back to C57BL/6J coordinates by running Lapels (Huang *et al*., 2014). All unpaired reads were then resorted by query name with samtools view -n and their flags were fixed with samtools fixmate. Informative reads (i.e. those that overlapped SNPs) were subsetted with the extractasReads.R utility from asSeq (Sun 2012) and remapped to the reciprocal genome using the same commands

as above. To retrieve our final set of allele-specific reads, we inputted the informative reads into the WASP pipeline (van de Geijn *et al*., 2015) to retain only those reads that map to a single locus in only one genome. Tag directories for both alleles were generated with HOMER's makeTagDirectory command with total mapped reads (i.e. before running WASP pipeline) and allele-specific reads.

For visualization purposes, mapped reads in .bam format were also converted to .bed format, and unique reads were retained (with sort -k1,1 -k2,2n -k3,3n -u) and extended by 150 bp with bedtools slop -l 0 -r 150. All samples were normalized to a depth of 10 million reads, and read coverage was calculated by bedtools genomeCoverageBed. The output .bedgraph file was then converted with UCSC's bedGraphtobigWig utility, and all tracks displayed were visualized with the UCSC Genome Browser (GRCm38/mm10).

ATAC-seq peak calling

Reads from individual bioreplicates were pooled with samtools merge. Two pseudoreplicates consisting of a random subset (50%) of total reads were generated by samtools view -h -b -s 1.5 and samtools view -h -b -s 2.5. Peaks were called from pooled reads and from two psuedoreplicates using macs2 (Liu 2014) with the following options: -p 1e-1 --nomodel --extsize 200. Peaks were also called using spp (Kharchenko *et al*., 2008) with -npeak=500000 to include a large set of putative peaks. For both macs2 and spp, reads from input DNA pooled from all ChIP-seq experiments were used as the control sample. To analyze consistency of peak calling across

pseudoreplicates, we employed an Irreproducible Discovery Rate (IDR) approach (Landt *et al*., 2012) by running batch-consistency-analysis.R and ranking peaks by p.value for macs2 and signal.value for spp. Peaks with a global IDR score of 0.0025 or less were retained for downstream analyses. Since peaks called across samples from different genotypes can vary somewhat in their specific coordinates, we generated a total universe of possible ATAC-seq peaks by combining all sequencing reads into a single tag directory in HOMER (Heinz et al., 2010). We then used the HOMER function getPeakTags with the -center option to generate single bp coordinates with maximal ATAC-seq signal (which we refer to in our manuscript as ATAC-seq summits).

Allele-specific CUT&RUN peak calling

Peak calling was performed as detailed above for ATAC-seq data, except reads mapping to the C57BL/6J and corresponding pseudogenome for each F_1-hybrid line were inputted separately into macs2 and spp. CUT&RUN peaks were then intersected with all ATAC summits detected across all genotypes and were recentered on the summit of ATAC-seq signal. This was important to do because peak calling algorithms that we used would often identify multiple histone modification peaks for individual CREs due to the non-continuous enrichment in signal. This also enabled us to generate uniform windows centered around ATAC-seq summits to consistently quantify signal for CUT&RUN data across different ATAC-seq summits. Peaks from both the C57BL/6J and pseudogenome were concatenated, and only peaks with at least one SNP/indel within +/- 60 bp of the ATAC summit were retained for allele-specific analysis (as highly “mappable” sites). To determine whether the CUT&RUN signal is significantly skewed

towards one allele, we used HOMER (Heinz *et al*., 2010) to annotate read coverage with -noadj -size -250,250 for AP-1 and -noadj -size -500,500 for H3K27ac. These counts were inputted in DESeq2 (Love *et al*., 2014), and all peaks with an FDR < 0.1 were considered allele-specific. Both allele-specific and shared peaks were then filtered by the following criteria: (1) when peak summits occurred within 1 kb of one another, only the summit with the highest pooled ATAC-seq signal was retained for downstream analyses, (2) peaks within the bottom quintile of pooled ATAC-seq signal per condition per F1-hybrid line were also excluded as low-signal sites, and (3) peaks that fell within 100 kb of gene bodies of known imprinted genes were filtered out of our remaining dataset to rule out differences in CRE activity that result from parent-of-origin effects (Shen *et al*., 2014).

Validation of CUT&RUN experiments

Since we modified existing protocols for CUT&RUN (Skene and Henikoff, 2017) to decrease the number of cells and sequencing reads compared to those typically required for generating ChIP-seq data, we performed a series of analyses to ensure that we were still able to quantitatively measure TF binding. While other MNase-based methods have reported sequence-dependent biases that could result in preferential cutting at open chromatin regions (Chung *et al*., 2010), we noted a similar fraction of reads in peaks from CUT&RUN and ChIP-seq when using identical antibodies (**Figure 3 – figure supplement 2D**), suggesting that we observe a minimal open chromatin bias with our modified CUT&RUN protocol. We also noted similar levels of binding at Fos peaks with ChIP-seq using our newly generated Fos antibody in comparison with a

previously available commercial antibody, and we confirmed the specificity of our antibody by comparing peaks found in our Fos-binding data with HA ChIP-seq data from wild-type C57BL/6J MEFs and C57BL/6J MEFs that express Fos-FLAG-HA (**Figure 3 – figure supplement 2A-C**). When we computationally separate shorter (<120 bp) from nucleosomal (>150 bp) Fos CUT&RUN reads, we found that sub-nucleosomal reads were more likely to be enriched at the core of Fos-bound enhancers, showed greater signal-to-noise relative to an IgG control antibody (**Figure 3 – figure supplement 2F**), and could be used to detect footprints containing AP-1-binding motifs (as a proxy for the detection for sequence-specific AP-1 binding; **Figure 3 – figure supplement 2G**).

Motif footprinting with CUT&RUN reads

Since CUT&RUN utilizes an antibody-targeted MNase for cleaving DNA fragments at TF-bound regions, individual cut sites derived from both ends of paired-end sequencing reads can be used for higher resolution mapping of specific nucleotides bound by TFs within peaks. DNA motifs that are recurrently protected (termed “footprints”) from MNase by chromatin-associated protein binding were identified from Fos CUT&RUN experiments performed in serum-stimulated C57BL/6J MEFs. Peak calling, motif identification, and footprinting analysis were performed using CUT&RUNtools (Zhu *et al*., 2019) with default parameters. Shown in **Figure 3 – figure supplement 2G** is the aggregated cut site probability within +/- 100 bp of all identified MTGAGTCA sites at Fos CUT&RUN peaks, suggesting that our Fos CUT&RUN experiments are able to detect direct binding sites for AP-1.

Allele-specific ChIP-seq peak calling

Peak calling was performed as detailed above for CUT&RUN data, except we considered all ChIP-seq peaks that overlapped ATAC-seq summits. All experiments (except for CTCF ChIP-seq, which was done in cycling cells) were performed in serum-starved and restimulated MEFs (90 min) and peaks from these datasets were analyzed separately and subsequently combined for downstream analyses, with the exception of experiments that directly queried enriched motifs at stimulus-responsive enhancers (Figure 3 – figure supplement 1B). We merged peak sets across timepoints due to the similar dynamics of enhancer activity observed across a more extensive serum stimulation timecourse in MEFs, with ~83% of enhancers exhibiting similar H3K27ac signal at 0, 10, and 90 min (Vierbuchen *et al*., 2017). Similarly, we merged our Tead1 binding data across 0 min and 90 min conditions to include as many binding sites as possible for motif analyses. This was not performed for Fos because we observed zero significant Fos peaks genome-wide in serum-starved MEFs, consistent with the fact that Fos protein is virtually undetectable in serum-starved MEFs.

Detection of significant Hi-ChIP interactions

H3K27ac Hi-ChIP reads were aligned with HiC-Pro (Servant *et al*., 2015) using an MboI-digested mm10 genome as the reference genome. Significant H3K27ac loops were determined by running hichipper (Lareau and Aryee, 2018), inputting 1 kb windows centered on all previously identified distal active enhancers from C57BL/6J MEFs (Vierbuchen *et al*., 2017) as possible loop anchors. Only loops that were supported by at least 10 paired-end tags per replicate and had a p-value < 1e-4 from

hichipper were retained from each timepoint (0m and 90m). Using these criteria, we noted similar numbers of H3K27ac Hi-ChIP loops in our dataset as those from other cell types (Mumbach *et al*., 2017). We generated tracks for visualization by retaining the midpoint of all significant loops.

Analysis of allele-specific gene expression

Reads were mapped with STAR 2.7.3 (Dobin *et al*., 2013) with the following options to enable WASP filtering of allele-specific reads: --outSAMattributes NH HI AS nM vG vA --waspOutputMode SAMtag. Genome-specific reads were extracted and converted into .bam format with samtools view -h -b -F 3844 -q 10. The featureCounts command from Subread (Liao *et al*., 2013) was used to quantify the number of allele-specific reads per genome that overlapped each mm10 Refseq gene bodies. Genes with an average expression per sample < 1 were filtered out, and counts from individual genotypes and timepoints were inputted into edgeR. Genes with an FDR < 0.05 by glmQLFTest were considered allele-specific in their expression.

Scatterplots for quantifying TF binding or chromatin state across alleles

Allele-specific reads are converted from .bam files into tag directories for HOMER (Heinz *et al*., 2010). Single bp coordinates, typically from ATAC-seq summits, are annotated with separate tag directories for the C57BL/6J and pseudogenome-specific reads with the following options: mm10 -noadj -size -250,250 for TFs and mm10 -noadj -size -500,500 for histone modifications. The resulting read coverage values are log2 transformed and plotted with geom_point in ggplot2 against one another.

Aggregate plots for averaging TF binding or chromatin state across peaks

Allele-specific reads were prepared as described above with HOMER. ATAC-seq peak centers or TF motif k-mers were then annotated with allele-specific read tag directories with the following options: mm10 -noadj -noann -nogene -size -1000,1000 -hist 10. Individual coverage values across 10 bp bins are plotted with geom_line in ggplot2.

Number and position of SNPs/indels at *cis*-regulatory elements

To determine the total number of SNPs/indels within the central 150 bp of enhancers as in **Figure 2I**, we used bedtools window -w 75 -c and centered on the ATAC-seq summit present at each putative CRE. We also mapped the positioning of SNPs/indels relative to the ATAC-seq summit by using bedtools window -w 200, and computed the difference in coordinates between the ATAC-seq summit and the closest nucleotide present in the SNP/indel. For defining the locations of putative CTCF motifs, we inputted the MA0139.1 profile from the JASPAR database into FIMO and limited the maximum stored scores to 10^6 per genome. The density of SNPs/indels at regions with significant allele-specific signal was visualized (as in **Figure 2H-J** and **Figure 5A-F**) using the geom_histogram function with default parameters (from ggplot2), after centering upon the given coordinate of interest indicated on the horizontal axis. On these same plots, we plotted the smoothed density estimates for sites with allele-specific (black trace) and shared (blue trace) using the geom_density function (from ggplot2).

Mammalian conservation scores at *cis*-regulatory elements

To more directly compare allele-specific and shared CREs with similar levels of transcriptional activity, we subsampled the pool of shared CREs such that the distribution of H3K27ac levels (+/- 500 bp from ATAC-seq summit) on the active allele matched that of the allele-specific CREs. Bigwig files with phastCons scores for 60 vertebrate species for each mouse mm10 chromosome were obtained from UCSC. For each CRE, we computed a phastCons score for a 150 bp window centered on the ATAC-seq summit using the bigWigAverageOverBed script from UCSC Tools (Version 3.6.3).

Identifying recurrent k-mer clusters at *cis*-regulatory elements with KMAC

Nucleotide sequences present at the central 60 bp of enhancers were extracted using bedtools getfasta (Quinlan and Hall, 2010). These .fasta files were inputted into KMAC (Guo *et al*., 2018) as the positive sequences (using the appropriate --k_seqs [n]) and enriched k-mer clusters are determined relative to random GC-matched control regions of equal length from the C57BL/6J genome (using --gc -1) with the following additional options: --k_min 5 --k_max10 --k_top 10.

Identifying k-mers that distinguish classes of AP-1 bound sites with gkm-SVM

Coordinates for AP-1 peaks were converted to appropriate pseudogenome coordinates with modmap (Huang *et al*., 2014) with -f and -d options. Nucleotide sequences in .fasta format for both alleles of each locus (60 bp window) were obtained with bedtools getfasta and were concatenated across different F_1-hybrid lines. For performing the active versus inactive Fos-bound site comparison, we used the gkm-SVM package

developed by Dr. Michael Beer's lab (Ghandi *et al*., 2016) and generated the kernel matrix by inputting the active allele DNA sequence (with higher H3K27ac levels) as the positive set and the corresponding inactive allele DNA sequence as the negative set. SVM training was done with the gkmsvm_trainCV command using default parameters and k-mer weights were calculated for all possible 10-mers with gkmsvm_classify.

ACKNOWLEDGEMENTS

We would like to thank members of the Greenberg Lab for their scientific advice and input throughout this project, L. Hu for assistance in generating the anti-Fos antibody used in this study, and S. Bhunia for help with data visualization. We are grateful to L. Boxer, A. Carter, C. Davis, E. Duffy, E. Griffith, and E. Li for their helpful feedback on this manuscript.

M.G.Y. was supported by National Institutes of Health under training grants T32EY00711030 and T32AG000222. E.L. was supported by the National Science Foundation Graduate Research Fellowship under grant numbers DGE0946799 and DGE1144152. This work was funded by the NIH (R01 NS115965 to M.E.G.).

DATA AVAILABILITY

All genomic data reported in this study have been deposited in the NCBI Gene Expression Omnibus (GSE193728).

DECLARATION OF INTERESTS

The authors declare no competing interests.

FIGURE LEGENDS

Figure 1. Allele-specific mapping of CREs and TF binding.

(A) F_1-hybrid male MEFs were derived from crosses between female C57BL/6J mice and male mice from a panel of inbred mouse strains. Experiments were performed in quiescent (0 min) and serum-stimulated (90 min) MEFs from at least two independent male embryos as biological replicates for each assay. Reads were mapped to either the maternal or paternal allele to quantify chromatin state and TF binding at CREs in an allele-specific manner. For wild-derived inbred strains, ATAC-seq data was generated using MEFs from corresponding parental lines and compared with chromatin accessibility in C57BL/6J MEFs. Similarly, H3K27ac Hi-ChIP data was obtained only from starved and serum-stimulated MEFs from C57BL/6J mice. All other genomic data indicated herein were obtained using MEFs derived from male F_1-hybrid embryos. (**B)** Example genome browser track of a locus (chr5:147,587,473-147,599,697 in mm10 genome) with an allele-specific enhancer (indicated in gray, on the right) in C57BL/6J x SPRET/EiJ F_1-hybrid MEFs. Normalized read densities for ATAC-seq and H3K27ac ChIP-seq for each allele are shown. (**C-F)** Scatterplots of maternal (C57BL/6J) and paternal allele-specific signal for histone modifications and CTCF binding (n = 61,288 proximal H3K27ac, n = 138,662 distal H3K27ac, n = 47,485 distal CTCF, n = 46,853 proximal H3K4me3, n = 127,077 distal H3K4me1, and n = 97,084 distal H3K4me2 allele pairs, respectively). Points indicated in light and dark colors represent peaks with and

without a significant skew in signal between alleles, respectively (FDR < 0.1 with DESeq2). CTCF and H3K4me3 levels were less likely to show an allele-specific skew in signal, in comparison with H3K27ac levels at active enhancers (Fisher's exact test, $p < 2.2 \times 10^{-16}$ for CTCF, $p < 2.2 \times 10^{-16}$ for H3K4me3). **(G)** Scatterplot of allele-specific H3K4me1, ATAC-seq, and Fos binding signal at top decile of allele-specific enhancers, comparing signal from the active and inactive alleles (defined based on relative H3K27ac levels) to one another (n = 13,862 allele pairs).

Figure 2. Number and position of genetic variants at allele-specific CREs. (A) Schematic depicting TF-bound enhancer with zero SNPs/indels (denoted by red X's) in the transposase-accessible CRE region (indicated in orange). Nucleosomes flanking both ends of the accessible region at active enhancers are marked by histone post-translational modifications, which are used as proxies for the transcriptional state of each enhancer. DNA sequences in these flanking regions tend to also be less conserved that sequences within enhancers themselves, thus often allowing sequencing reads to be correctly assigned to one of two genomes in F_1-hybrid cells in the absence of SNPs/indels within enhancer sequences. **(B)** Example genome browser track of a locus (chr11:113,290,106-113,416,149 (top) and chr11:113,350,775-113,356,042 (bottom) in mm10 genome) with an allele-specific 0-SNP/indel enhancer (indicated in gray, on the left) within an enhancer "cluster" in C57BL/6J x CAST/EiJ F_1-hybrid MEFs. The 0-SNP enhancer is situated <2 kb from a SNP/indel-containing enhancer (indicated in green) within the same cluster. Normalized read densities for ATAC-seq and H3K27ac ChIP-seq for each allele are

shown. Tick marks indicate positions of annotated SNPs/indels that distinguish the C57BL/6J and CAST/EiJ genomes. **(C-E)** Histogram of number of SNPs/indels present within the central 150 bp of allele-specific and signal-matched, shared active enhancers, promoters, and putative insulators (mean = 2.36 and 1.57 SNPs/indels for enhancers, respectively, two-tailed unpaired t-test, $p < 2.2 \times 10^{-16}$ for enhancers; mean = 1.84 and 1.09 SNPs/indels for promoters, respectively; two-tailed unpaired t-test, $p = 7.9 \times 10^{-4}$ for promoters; mean = 2.95 and 2.03 SNPs/indels for insulators, respectively; two-tailed unpaired t-test, $p < 2.2 \times 10^{-16}$ for insulators). Shared enhancers were randomly subsampled such that they were signal-matched to the active allele signal from the total set of allele-specific enhancers. (**F)** Proportion of enhancers that show allele-specific and >2-fold difference in signal, plotted as a function of the number of SNPs/indels present within their central 150 bp. Shared enhancers were randomly subsampled such that they were signal-matched to the active allele signal from the total set of allele-specific enhancers. (**G)** Box and whisker plot of H3K27ac fold changes between active and inactive alleles for allele-specific enhancers and promoters, plotted as a function of the number of SNPs/indels present within their central 150 bp. **(H-J)** Frequency of SNPs/indels at positions relative to ATAC-seq summits for allele-specific (and >2-fold) versus signal-matched, shared active enhancers, 1-SNP active enhancers, and H3K4me3-marked promoters (Pearson's Chi-squared test, $p < 2.2 \times 10^{-16}$ for enhancers, $p = 5.4 \times 10^{-5}$ for 1-SNP enhancers, $p = 2.6 \times 10^{-9}$ for promoters). Mean number of SNPs within central 150 bp of enhancers: 4.468 for enhancers with allele-specific H3K27ac levels, 3.203 for signal-matched enhancers with shared H3K27ac levels.

Figure 3. Sequence motifs and changes in chromatin state at allele-specific TF-bound sites. (A-B) Scatterplots of maternal (C57BL/6J) and paternal allele-specific signal for AP-1 and TEAD binding (n = 85,198 distal Fos, and 75,350 distal Tead1 allele pairs, respectively). Points indicated in light and dark colors represent peaks with and without a significant skew in signal between alleles, respectively (FDR < 0.1 with DESeq2). **(C-D)** Distribution of SNPs centered on respective k-mers (denoted by dashed lines) at allele-specific, active, and gene-distal Fos and Tead1 peaks with >2-fold difference in binding signal across alleles (n = 263 and n = 1,035 allele pairs, respectively). **(E)** Distribution of SNPs centered on CTCF PWM (JASPAR matrix ID MA0139.1; denoted by dashed lines) at allele-specific, gene-distal CTCF peaks with >2-fold difference in binding signal across alleles (n = 1,663 allele pairs). **(F-I)** Aggregate plot of allele-specific Fos, ATAC-seq, H3K4me1, and H3K27ac reads centered on ATAC-seq summits at active Fos peaks. These sites have been selected because they contain a single SNP/indel-containing AP-1 site and no shared AP-1 sites within 75 bp of the ATAC-seq summit. Signal is compared between alleles with intact versus mutated core AP-1 motifs (TGASTCA; n = 1,307 allele pairs). **(J-M)** Aggregate plot of allele-specific Tead1, ATAC-seq, H3K4me1, and H3K27ac reads centered on ATAC-seq summits at active Tead1 peaks. These sites have been selected because they contain a single SNP/indel-containing TEAD site and no shared TEAD sites within 75 bp of the ATAC-seq summit. Signal is compared between alleles with intact versus mutated core TEAD motifs (GGAATK; n = 1,132 allele pairs).

Figure 4. Mechanisms of hierarchical binding for AP-1 and TEAD TFs. (A) Percentage of allele-specific (n = 1,635 allele pairs) versus shared (n = 142,778 allele pairs) gene-distal Fos peaks that contain strain-specific core AP-1 (TGASTCA; Fisher's exact test, $p < 2.2 \times 10^{-16}$) or extended TEAD (GGAATK; Fisher's exact test, $p = 2.123 \times 10^{-9}$) k-mer(s) within 75 bp of their respective ATAC-seq summits. **(B)** Percentage of allele-specific (n = 9,416 allele pairs) versus shared (n = 65,934 allele pairs) gene-distal Tead1 peaks that contain strain-specific core AP-1 (TGASTCA; Fisher's exact test, $p < 2.2 \times 10^{-16}$) or extended TEAD (GGAATK; Fisher's exact test, $p < 2.2 \times 10^{-16}$) k-mer(s) within 75 bp of their respective ATAC-seq summits. **(C)** Percentage of AP-1-only (n = 15,709 loci) peaks versus AP-1/TEAD co-bound peaks (n = 2,797 loci) in the C57BL/6J genome with at least one bindable AP-1 k-mer (VTGACTCB, VTGAATCAB, or VTTAGTCAY) present within 50 bp of their respective ATAC-seq summits (Fisher's exact test, $p < 2.2 \times 10^{-16}$). **(D)** Percentage of TEAD-only (n = 2,541 loci) peaks versus AP-1/TEAD co-bound peaks in the C57BL/6J genome with at least one extended TEAD k-mer (GGAATK) present within 50 bp of their respective ATAC-seq summits (Fisher's exact test, $p = 2.406 \times 10^{-9}$).

Figure 5. Distribution of genetic variants that influence AP-1, TEAD, and CTCF binding. (A-C) Frequency of SNPs/indels at positions relative to ATAC-seq summits at allele-specific (with >2-fold difference in signal between alleles) versus shared gene-distal Fos, Tead1, and CTCF peaks (Pearson's Chi-squared test, $p = 9.7 \times 10^{-8}$ for AP-1, $p < 2.2 \times 10^{-16}$ for TEAD, $p < 2.2 \times 10^{-16}$ for CTCF, 100 bp window centered on ATAC-seq summit in all cases). **(D-E)** Frequency of SNPs/indels at positions relative to shared

VTGACTCAB and GGAATK k-mers within 75 bp of the ATAC-seq summit at allele-specific (with >2-fold difference in signal between alleles) versus shared gene-distal Fos and Tead1 peaks, respectively. Sites have been filtered to exclude any peaks that include SNPs/indels that overlap their cognate k-mers. **(F)** Frequency of SNPs/indels at positions relative to shared CTCF PWM (MA0139.1) within 75 bp of the ATAC-seq summit at allele-specific (with >2-fold difference in signal between alleles) versus shared gene-distal CTCF peaks. Sites have been filtered to exclude any peaks that include SNPs/indels at disrupt the CTCF PWM in a strain-specific manner.

Figure 6. Machine learning prediction of AP-1 binding sites genome-wide. (A-B) Area under ROC and P-R curves for gkm-SVM comparison of Fos peaks in the C57BL/6J genome (positive set) and length-matched, random genomic regions (negative set). Shown are AUC values for different lengths of input DNA sequence, ranging from 10 to 300 bp, indicated in black. The same analysis was repeated after masking all instances of core AP-1 motifs (TGASTCA; n = 4,000 randomly selected loci), indicated in green. **(C)** Frequency of consensus, human DNase footprints (from Vierstra *et al*., 2020) containing an extended AP-1 k-mer (VTGACTCAB) at positions relative to DNase-seq summits (n = 164,705 footprints). **(D)** Width of DNase footprints that contain an extended AP-1 k-mer (VTGACTCAB). **(E)** Number of additional DNase footprints within 100 bp of DNase-seq summits at DNase peaks with a VTGACTCAB-containing footprint. **(F)** Distance between VTGACTCAB-containing footprints and nearest neighboring DNase footprint.

SUPPLEMENTAL FIGURE LEGENDS

Figure 1 – figure supplement 1. (**A)** Volcano plots of chromatin-associated RNA-seq read density at annotated gene bodies. Indicated on the horizontal axis is the ratio of allele-specific signal between paternal and maternal (C57BL/6J) alleles for each F_1-hybrid strain. Transcripts whose expression levels are significantly allele-specific in DEseq2 (FDR < 0.1) and edgeR (FDR < 0.05) are highlighted in blue. **(B)** (Left) Number of SNPs/indels annotated in each wild-derived inbred mouse strain, relative to the C57BL/6J genome. (Right) Number of transcripts per F_1-hybrid line with significant allele-specific expression from reads pooled across all timepoints (0, 20, and 90 min).

Figure 1 – figure supplement 2. (A) Percentage of primed CREs (ATAC-seq summits overlapping H3K4me1/2 peaks) identified in any F_1-hybrid strain that are active regulatory elements (overlap H3K27ac peaks). In total, we found n = 283,339 pairs of active CRE alleles across all F_1-hybrids in our dataset, including n = 142,898 pairs that contained SNP(s) within the central 120 bp relative to their respective ATAC-seq summits, which we considered to be highly mappable sites. **(B)** Percentage of active CREs with a significant skew in H3K27ac levels between alleles, which we denoted as allele-specific enhancers or promoters (based on distance to their nearest annotated TSS) for subsequent analyses (n = 31,627/138,622 allele pairs; FDR < 0.1 with DEseq2). **(C)** Distance to nearest annotated TSS for active CREs identified in any F_1-hybrid strain (median = 19,786 bp). CREs were considered gene-distal if they occurred >1 kb from the nearest annotated TSS (cutoff denoted by dashed line). **(D)** Percentage

of active enhancers that exhibit an allele-specific skew in nascent transcription levels for putative target genes, which were identified by statistically significant H3K27ac Hi-ChIP loops formed with active promoters that overlap an annotated TSS. Allele-specific enhancers are more likely than enhancers with shared H3K27ac signal to be linked with allele-specific transcripts (n = 1,002/6,907 and n = 3,403/37,390 detectable Hi-ChIP loops for allele-specific and shared enhancers, respectively; Fisher's exact test, $p = 2.2 \times 10^{-16}$).

Figure 2 – figure supplement 1. (A) Distribution of H3K27ac signal from the active allele at (1) allele-specific enhancers, (2) all shared enhancers, and (3) a randomly subsampled set of shared enhancers that were signal-matched to the active allele of allele-specific sites. **(B)** Frequency of SNPs/indels for enhancers in our dataset assigned as 0-SNP/indel enhancers, which we defined as those having no annotated genetic variants within 75 bp of the ATAC-seq summit. No notable differences in the pattern of SNPs/indels were observed between allele-specific (black trace) and shared (blue trace) 0-SNP enhancers in regions flanking the central 150 bp window that contains no genetic variants. **(C-E)** Cumulative distribution of distances to nearest allele-specific CTCF peak, nearest allele-specific CRE, and nearest active CRE. Shown is a comparison between allele-specific and signal-matched, shared enhancers, and both sets of sites contain zero SNPs/indels in their central 150 bp (Kolmogorov-Smirnov, p = 0.0142 for nearest allele-specific CTCF peak; Kolmogorov-Smirnov D = 0.02788 for nearest allele-specific CTCF peak; p < 0.0001 for nearest allele-specific CRE; Kolmogorov-Smirnov D = 0.1313 for nearest allele-specific CRE; p < 0.0001 for

nearest active CRE; Kolmogorov-Smirnov D = 0.05563, for nearest active CRE). **(F)** Cumulative distribution of phastCons scores for allele-specific and signal-matched, shared active enhancers and promoters (Kolmogorov-Smirnov, $p < 0.0001$ and Kolmogorov-Smirnov D = 0.1274 for enhancers; Kolmogorov-Smirnov, $p < 0.0001$ and Kolmogorov-Smirnov D = 0.1137 for promoters).

Figure 2 – figure supplement 2. (A) Scatterplot of H3K27ac CUT&RUN signal at active CREs identified on the X-chromosome of the C57BL/6J x 129/SvImJ F_1 hybrid (n = 216 peaks). Shown are pairwise comparisons of H3K27ac read densities from the C57BL/6J x 129/SvImJ line and normalized H3K27ac CUT&RUN signal from other F_1-hybrid lines. Since we set up our breeding scheme such that each F_1-hybrid MEF line was derived only from male embryos that contain a single X-chromosome inherited from their C57BL/6J mother, this enabled us to quantify chromatin state without the need for allele-specific mapping at this particular set of CREs. **(B)** Scatterplot of nascent RNA-seq read counts overlapping gene bodies of expressed transcripts on the C57BL/6J X-chromosome (with an average of at least 100 reads per F_1-hybrid line). For example, amongst 427 expressed genes on the X-chromosome, we found that n = 39 (9.3%) were expressed with >2-fold difference in signal between alleles, when comparing the C57BL/6J x CAST/EiJ and the C57BL/6J x SPRET/EiJ F_1 hybrids.

Figure 3 – figure supplement 1. (A) Top enriched k-mer clusters identified with the KMAC algorithm present in the top decile of active C57BL/6J enhancers (Guo *et al*., 2018). DNA sequence from central 60 bp of enhancer regions were compared with

random GC- and length-matched regions in the C57BL/6J genome. AP-1 k-mers were present in n = 1,410/4,579 active enhancers and n = 74/4,579 control regions, respectively. TEAD k-mers were present in n = 499/4,579 active enhancers and n = 29/4,579 control regions, respectively. **(B)** Top enriched k-mer clusters identified with the KMAC algorithm present in late-response gene enhancers in the C57BL/6J genome. Control regions used for comparison were constitutively active enhancers in the C57BL/6J genome. **(C)** Percentage of allele-specific versus shared Fos peaks that contain an extended AP-1 motif (VTGACTCAB) with a SNP in the 3 bp flanking the core motif (TGACTCA; Fisher's exact test, $p = 5.2 \times 10^{-3}$).

Figure 3 – figure supplement 2. (A) Scatterplot of Fos ChIP-seq read density at Fos peaks originally identified in C57BL/6J MEFs, comparing signal from commercial (Santa Cruz Biotechnology sc-7202X) and in-house generated Fos (1096AE) antibodies. **(B)** Scatterplot of read density at Fos peaks originally identified in C57BL/6J MEFs, comparing signal from Fos and HA ChIP-seq experiments performed in MEFs expressing an epitope-tagged form of Fos (Fos-FLAG-HA). **(C)** Scatterplot of HA ChIP-seq read density at Fos peaks originally identified in C57BL/6J MEFs, comparing signal in wild-type C57BL/6J MEFs and Fos-FLAG-HA MEFs. **(D)** Fraction of mapped reads in C57BL/6J MEFs that fall within Fos and H3K27ac peaks (500 bp and 1 kb windows, respectively). Identical antibodies were used for ChIP-seq and CUT&RUN experiments. **(E)** Fragment lengths for mappable paired-end Fos and H3K27ac CUT&RUN reads (median = 139 and 163 bp, respectively). **(F)** Aggregate plot of Fos CUT&RUN reads mapped to the C57BL/6J genome, pooled from data across five F_1-hybrid lines, and

centered on ATAC-seq summits at Fos peaks originally identified in C57BL/6J MEFs. Paired-end reads are categorized based on fragment size as either sub-nucleosomal (<120 bp) or nucleosomal (>150 bp). **(G)** MNase cut site probability for Fos CUT&RUN reads defined using CUT&RUNTools (Zhu *et al*., 2019) identifies a TF footprint centered on MTGAGTCA k-mer at Fos peaks, suggesting that our CUT&RUN data can reliably identify instances of direct AP-1 binding.

Figure 6 – figure supplement 1. (A-C) ROC and P-R curves for gkm-SVM comparison of Fos, Tead1, and CTCF peaks compared to randomly sampled regions in the C57BL/6J genome. **(D-G)** Top enriched 10-mers from gkm-SVM comparing the central 60 bp from n = 4,000 randomly selected Fos (with and without masking TGASTCA k-mers), Tead1, and CTCF peaks in C57BL/6J MEFs (positive set) with n = 4,000 randomly sampled 60 bp windows across the C57BL/6J genome (negative set). **(H)** Top enriched 10-mers from gkm-SVM comparing the central 60 bp from active (positive set) and inactive allele (negative set) at Fos peaks with significantly allele-specific H3K27ac levels. **(I)** Top enriched 10-mers from gkm-SVM comparing the central 60 bp from n = 4,000 DNase footprints containing VTGACTCAB k-mers (positive set) and n = 4,000 random gene-distal genomic windows in the human genome (hg38) centered on VTGACTCAB k-mers (negative set).

SUPPLEMENTARY FILE LEGENDS

Supplementary File 1. Total numbers of SNPs/indels per inbred mouse strain relative to the C57BL/6J reference strain. ATAC-seq peaks were considered highly mappable if they contained a SNP/indel within a 120 bp window centered on their respective ATAC-seq summits.

Supplementary File 2. Experimental condition, replicate number, number of sequencing reads, and percentage of non-duplicated reads for all genomic assays performed in this study.

Supplementary File 3. List of all significant H3K27ac Hi-ChIP loops at 0 or 90 min serum stimulation in wild-type C57BL/6J MEFs ($p < 1e-4$). Only intra-chromosomal loops with at least 10 paired-end reads connecting them per bioreplicate were retained for analysis.

Supplementary File 4. Number of allele pairs with allele-specific and shared signal for each transcription factor or histone modification surveyed in our dataset. For Fos and H3K27ac experiments, the data from ChIP-seq (wild-derived inbred strains; CAST/EiJ, MOLF/EiJ, PWK/PhJ, SPRET/EiJ) and CUT&RUN (less divergent inbred strains; 129S1/SvImJ, A/J, BALB/cJ, DBA/2J, NOD/ShiLtJ) were merged in all rows designated "all strains". Only CUT&RUN peaks with a SNP/indel present within 60 bp of the ATAC-seq summit were included for allele-specific analyses for non-wild-derived (i.e. less genetically divergent) strains.

Supplementary File 5. Significant allele-specific transcripts from chromatin-associated RNA-seq data using reads pooled from 0, 20, and 90 min timepoints. Positive and negative fold-changes indicate genes expressed at higher levels on the paternal, wild-derived allele and maternal, C57BL/6J allele, respectively.

Supplementary File 6. Location, allele-specific H3K27ac values, and DNA sequences for top decile of allele-specific enhancers, with greatest fold-change in H3K27ac signal between active and inactive alleles.

REFERENCES

Albert, F. W., & Kruglyak, L. (2015). The role of regulatory variation in complex traits and disease. *Nature Reviews. Genetics*, *16*(4), 197–212. https://doi.org/10.1038/nrg3891

Arnold, C. D., Gerlach, D., Stelzer, C., Boryń, Ł. M., Rath, M., & Stark, A. (2013). Genome-wide quantitative enhancer activity maps identified by STARR-seq. *Science (New York, N.Y.)*, *339*(6123), 1074–1077. https://doi.org/10.1126/science.1232542

Arnosti, D. N., & Kulkarni, M. M. (2005). Transcriptional enhancers: Intelligent enhanceosomes or flexible billboards?. *Journal of Cellular Biochemistry*, *94*(5), 890–898. https://doi.org/10.1002/jcb.20352

Avsec, Ž., Weilert, M., Shrikumar, A., Krueger, S., Alexandari, A., Dalal, K., Fropf, R., McAnany, C., Gagneur, J., Kundaje, A., & Zeitlinger, J. (2021). Base-resolution models of transcription-factor binding reveal soft motif syntax. *Nature Genetics*, *53*(3), 354–366. https://doi.org/10.1038/s41588-021-00782-6

Barozzi, I., Simonatto, M., Bonifacio, S., Yang, L., Rohs, R., Ghisletti, S., & Natoli, G. (2014). Coregulation of transcription factor binding and nucleosome occupancy through DNA features of mammalian enhancers. *Molecular Cell*, *54*(5), 844–857. https://doi.org/10.1016/j.molcel.2014.04.006

Bevington, S. L., Cauchy, P., Piper, J., Bertrand, E., Lalli, N., Jarvis, R. C., Gilding, L. N., Ott, S., Bonifer, C., & Cockerill, P. N. (2016). Inducible chromatin priming is associated with the

establishment of immunological memory in T cells. *The EMBO Journal*, *35*(5), 515–535. https://doi.org/10.15252/embj.201592534

Biddie, S. C., John, S., Sabo, P. J., Thurman, R. E., Johnson, T. A., Schiltz, R. L., Miranda, T. B., Sung, M. H., Trump, S., Lightman, S. L., Vinson, C., Stamatoyannopoulos, J. A., & Hager, G. L. (2011). Transcription factor AP1 potentiates chromatin accessibility and glucocorticoid receptor binding. *Molecular Cell*, *43*(1), 145–155. https://doi.org/10.1016/j.molcel.2011.06.016

Bilu, Y., & Barkai, N. (2005). The design of transcription-factor binding sites is affected by combinatorial regulation. *Genome Biology*, *6*(12), R103. https://doi.org/10.1186/gb-2005-6-12-r103

Bogdanovic, O., Fernandez-Miñán, A., Tena, J. J., de la Calle-Mustienes, E., Hidalgo, C., van Kruysbergen, I., van Heeringen, S. J., Veenstra, G. J., & Gómez-Skarmeta, J. L. (2012). Dynamics of enhancer chromatin signatures mark the transition from pluripotency to cell specification during embryogenesis. *Genome Research*, *22*(10), 2043–2053. https://doi.org/10.1101/gr.134833.111

Bolger, A. M., Lohse, M., & Usadel, B. (2014). Trimmomatic: a flexible trimmer for Illumina sequence data. *Bioinformatics (Oxford, England)*, *30*(15), 2114–2120. https://doi.org/10.1093/bioinformatics/btu170

Bonn, S., Zinzen, R. P., Girardot, C., Gustafson, E. H., Perez-Gonzalez, A., Delhomme, N., Ghavi-Helm, Y., Wilczyński, B., Riddell, A., & Furlong, E. E. (2012). Tissue-specific analysis of chromatin state identifies temporal signatures of enhancer activity during embryonic development. *Nature Genetics*, *44*(2), 148–156. https://doi.org/10.1038/ng.1064

Boyle, A. P., Davis, S., Shulha, H. P., Meltzer, P., Margulies, E. H., Weng, Z., Furey, T. S., & Crawford, G. E. (2008). High-resolution mapping and characterization of open chromatin across the genome. *Cell*, *132*(2), 311–322. https://doi.org/10.1016/j.cell.2007.12.014

Boyle, E. A., Li, Y. I., & Pritchard, J. K. (2017). An Expanded View of Complex Traits: From Polygenic to Omnigenic. *Cell*, *169*(7), 1177–1186. https://doi.org/10.1016/j.cell.2017.05.038

Buenrostro, J. D., Wu, B., Chang, H. Y., & Greenleaf, W. J. (2015). ATAC-seq: A Method for Assaying Chromatin Accessibility Genome-Wide. *Current Protocols in Molecular Biology*, *109*, 21.29.1–21.29.9. https://doi.org/10.1002/0471142727.mb2129s109

Bushnell, B. (2014). BBMap: A Fast, Accurate, Splice-Aware Aligner. *Lawrence Berkeley National Laboratory*. LBNL Report #: LBNL-7065E. Retrieved from https://escholarship.org/uc/item/1h3515gn

Carroll S. B. (2008). Evo-devo and an expanding evolutionary synthesis: a genetic theory of morphological evolution. *Cell*, *134*(1), 25–36. https://doi.org/10.1016/j.cell.2008.06.030

Chen, L., Loh, P. G., & Song, H. (2010). Structural and functional insights into the TEAD-YAP complex in the Hippo signaling pathway. *Protein & Cell*, *1*(12), 1073–1083. https://doi.org/10.1007/s13238-010-0138-3

Chung, H. R., Dunkel, I., Heise, F., Linke, C., Krobitsch, S., Ehrenhofer-Murray, A. E., Sperling, S. R., & Vingron, M. (2010). The effect of micrococcal nuclease digestion on nucleosome positioning data. *PloS One*, *5*(12), e15754. https://doi.org/10.1371/journal.pone.0015754

Comoglio, F., Simonatto, M., Polletti, S., Liu, X., Smale, S. T., Barozzi, I., & Natoli, G. (2019). Dissection of acute stimulus-inducible nucleosome remodeling in mammalian cells. *Genes & Development*, *33*(17-18), 1159–1174. https://doi.org/10.1101/gad.326348.119

Creyghton, M. P., Cheng, A. W., Welstead, G. G., Kooistra, T., Carey, B. W., Steine, E. J., Hanna, J., Lodato, M. A., Frampton, G. M., Sharp, P. A., Boyer, L. A., Young, R. A., & Jaenisch, R. (2010). Histone H3K27ac separates active from poised enhancers and predicts developmental state. *Proceedings of the National Academy of Sciences of the United States of America*, *107*(50), 21931–21936. https://doi.org/10.1073/pnas.1016071107

Danecek, P., Auton, A., Abecasis, G., Albers, C. A., Banks, E., DePristo, M. A., Handsaker, R. E., Lunter, G., Marth, G. T., Sherry, S. T., McVean, G., Durbin, R., & 1000 Genomes Project Analysis Group (2011). The variant call format and VCFtools. *Bioinformatics (Oxford, England)*, *27*(15), 2156–2158. https://doi.org/10.1093/bioinformatics/btr330

de Almeida, B. P., Reiter, F., Pagani, M., & Stark, A. (2022). DeepSTARR predicts enhancer activity from DNA sequence and enables the de novo design of synthetic enhancers. *Nature Genetics*, *54*(5), 613–624. https://doi.org/10.1038/s41588-022-01048-5

Deplancke, B., Alpern, D., & Gardeux, V. (2016). The Genetics of Transcription Factor DNA Binding Variation. *Cell*, *166*(3), 538–554. https://doi.org/10.1016/j.cell.2016.07.012

Ding, Z., Ni, Y., Timmer, S. W., Lee, B. K., Battenhouse, A., Louzada, S., Yang, F., Dunham, I., Crawford, G. E., Lieb, J. D., Durbin, R., Iyer, V. R., & Birney, E. (2014). Quantitative genetics of CTCF binding reveal local sequence effects and different modes of X-chromosome association. *PLoS Genetics*, *10*(11), e1004798. https://doi.org/10.1371/journal.pgen.1004798

Dobin, A., Davis, C. A., Schlesinger, F., Drenkow, J., Zaleski, C., Jha, S., Batut, P., Chaisson, M., & Gingeras, T. R. (2013). STAR: ultrafast universal RNA-seq aligner. *Bioinformatics (Oxford, England)*, *29*(1), 15–21. https://doi.org/10.1093/bioinformatics/bts635

Dorighi, K. M., Swigut, T., Henriques, T., Bhanu, N. V., Scruggs, B. S., Nady, N., Still, C. D., 2nd, Garcia, B. A., Adelman, K., & Wysocka, J. (2017). Mll3 and Mll4 Facilitate Enhancer RNA Synthesis and Transcription from Promoters Independently of H3K4 Monomethylation. *Molecular Cell*, *66*(4), 568–576.e4. https://doi.org/10.1016/j.molcel.2017.04.018

Erceg, J., Saunders, T. E., Girardot, C., Devos, D. P., Hufnagel, L., & Furlong, E. E. (2014). Subtle changes in motif positioning cause tissue-specific effects on robustness of an enhancer's activity. *PLoS Genetics*, *10*(1), e1004060. https://doi.org/10.1371/journal.pgen.1004060

Eferl, R., & Wagner, E. F. (2003). AP-1: a double-edged sword in tumorigenesis. *Nature Reviews. Cancer*, *3*(11), 859–868. https://doi.org/10.1038/nrc1209

Farh, K. K., Marson, A., Zhu, J., Kleinewietfeld, M., Housley, W. J., Beik, S., Shoresh, N., Whitton, H., Ryan, R. J., Shishkin, A. A., Hatan, M., Carrasco-Alfonso, M. J., Mayer, D., Luckey, C. J., Patsopoulos, N. A., De Jager, P. L., Kuchroo, V. K., Epstein, C. B., Daly, M. J., Hafler, D. A., … Bernstein, B. E. (2015). Genetic and epigenetic fine mapping of causal autoimmune disease variants. *Nature*, *518*(7539), 337–343. https://doi.org/10.1038/nature13835

Farley, E. K., Olson, K. M., Zhang, W., Rokhsar, D. S., & Levine, M. S. (2016). Syntax compensates for poor binding sites to encode tissue specificity of developmental enhancers. *Proceedings of the National Academy of Sciences of the United States of America*, *113*(23), 6508–6513. https://doi.org/10.1073/pnas.1605085113

Farrance, I. K., Mar, J. H., & Ordahl, C. P. (1992). M-CAT binding factor is related to the SV40 enhancer binding factor, TEF-1. *The Journal of Biological Chemistry*, *267*(24), 17234–17240.

Fudenberg, G., & Pollard, K. S. (2019). Chromatin features constrain structural variation across evolutionary timescales. *Proceedings of the National Academy of Sciences of the United States of America*, *116*(6), 2175–2180. https://doi.org/10.1073/pnas.1808631116

Fulco, C. P., Nasser, J., Jones, T. R., Munson, G., Bergman, D. T., Subramanian, V., Grossman, S. R., Anyoha, R., Doughty, B. R., Patwardhan, T. A., Nguyen, T. H., Kane, M., Perez, E. M., Durand, N. C., Lareau, C. A., Stamenova, E. K., Aiden, E. L., Lander, E. S., & Engreitz, J. M. (2019). Activity-by-contact model of enhancer-promoter regulation from thousands of

CRISPR perturbations. *Nature Genetics*, *51*(12), 1664–1669. https://doi.org/10.1038/s41588-019-0538-0

Ghandi, M., Mohammad-Noori, M., Ghareghani, N., Lee, D., Garraway, L., & Beer, M. A. (2016). gkmSVM: an R package for gapped-kmer SVM. *Bioinformatics (Oxford, England)*, *32*(14), 2205–2207. https://doi.org/10.1093/bioinformatics/btw203

Grossman, S. R., Zhang, X., Wang, L., Engreitz, J., Melnikov, A., Rogov, P., Tewhey, R., Isakova, A., Deplancke, B., Bernstein, B. E., Mikkelsen, T. S., & Lander, E. S. (2017). Systematic dissection of genomic features determining transcription factor binding and enhancer function. *Proceedings of the National Academy of Sciences of the United States of America*, *114*(7), E1291–E1300. https://doi.org/10.1073/pnas.1621150114

Grubert, F., Zaugg, J. B., Kasowski, M., Ursu, O., Spacek, D. V., Martin, A. R., Greenside, P., Srivas, R., Phanstiel, D. H., Pekowska, A., Heidari, N., Euskirchen, G., Huber, W., Pritchard, J. K., Bustamante, C. D., Steinmetz, L. M., Kundaje, A., & Snyder, M. (2015). Genetic Control of Chromatin States in Humans Involves Local and Distal Chromosomal Interactions. *Cell*, *162*(5), 1051–1065. https://doi.org/10.1016/j.cell.2015.07.048

Guo, Y., Tian, K., Zeng, H., Guo, X., & Gifford, D. K. (2018). A novel *k*-mer set memory (KSM) motif representation improves regulatory variant prediction. *Genome Research*, *28*(6), 891–900. https://doi.org/10.1101/gr.226852.117

Halow, J. M., Byron, R., Hogan, M. S., Ordoñez, R., Groudine, M., Bender, M. A., Stamatoyannopoulos, J. A., & Maurano, M. T. (2021). Tissue context determines the penetrance of regulatory DNA variation. *Nature Communications*, *12*(1), 2850. https://doi.org/10.1038/s41467-021-23139-3

He, X., Chatterjee, R., John, S., Bravo, H., Sathyanarayana, B. K., Biddie, S. C., FitzGerald, P. C., Stamatoyannopoulos, J. A., Hager, G. L., & Vinson, C. (2013). Contribution of nucleosome binding preferences and co-occurring DNA sequences to transcription factor binding. *BMC Genomics*, *14*, 428. https://doi.org/10.1186/1471-2164-14-428

He, L., Pratt, H., Gao, M., Wei, F., Weng, Z., & Struhl, K. (2021). YAP and TAZ are transcriptional co-activators of AP-1 proteins and STAT3 during breast cellular transformation. *eLife*, *10*, e67312. https://doi.org/10.7554/eLife.67312

Heintzman, N. D., Stuart, R. K., Hon, G., Fu, Y., Ching, C. W., Hawkins, R. D., Barrera, L. O., Van Calcar, S., Qu, C., Ching, K. A., Wang, W., Weng, Z., Green, R. D., Crawford, G. E., & Ren, B. (2007). Distinct and predictive chromatin signatures of transcriptional promoters and enhancers in the human genome. *Nature Genetics*, *39*(3), 311–318. https://doi.org/10.1038/ng1966

Heinz, S., Benner, C., Spann, N., Bertolino, E., Lin, Y. C., Laslo, P., Cheng, J. X., Murre, C., Singh, H., & Glass, C. K. (2010). Simple combinations of lineage-determining transcription factors prime cis-regulatory elements required for macrophage and B cell identities. *Molecular Cell*, *38*(4), 576–589. https://doi.org/10.1016/j.molcel.2010.05.004

Heinz, S., Romanoski, C. E., Benner, C., Allison, K. A., Kaikkonen, M. U., Orozco, L. D., & Glass, C. K. (2013). Effect of natural genetic variation on enhancer selection and function. *Nature*, *503*(7477), 487–492. https://doi.org/10.1038/nature12615

Huang, S., Holt, J., Kao, C. Y., McMillan, L., & Wang, W. (2014). A novel multi-alignment pipeline for high-throughput sequencing data. *Database : The Journal of Biological Databases and Curation*, *2014*, bau057. https://doi.org/10.1093/database/bau057

Jadhav, U., Cavazza, A., Banerjee, K. K., Xie, H., O'Neill, N. K., Saenz-Vash, V., Herbert, Z., Madha, S., Orkin, S. H., Zhai, H., & Shivdasani, R. A. (2019). Extensive Recovery of Embryonic Enhancer and Gene Memory Stored in Hypomethylated Enhancer DNA. *Molecular Cell*, *74*(3), 542–554.e5. https://doi.org/10.1016/j.molcel.2019.02.024

Jang, Y., Wang, C., Zhuang, L., Liu, C., & Ge, K. (2017). H3K4 Methyltransferase Activity Is Required for MLL4 Protein Stability. *Journal of Molecular Biology*, *429*(13), 2046–2054. https://doi.org/10.1016/j.jmb.2016.12.016

Jindal, G. A., & Farley, E. K. (2021). Enhancer grammar in development, evolution, and disease: dependencies and interplay. *Developmental Cell*, *56*(5), 575–587. https://doi.org/10.1016/j.devcel.2021.02.016

Johnson, T. A., Chereji, R. V., Stavreva, D. A., Morris, S. A., Hager, G. L., & Clark, D. J. (2018). Conventional and pioneer modes of glucocorticoid receptor interaction with enhancer chromatin in vivo. *Nucleic Acids Research*, *46*(1), 203–214. https://doi.org/10.1093/nar/gkx1044

Jolma, A., Yin, Y., Nitta, K. R., Dave, K., Popov, A., Taipale, M., Enge, M., Kivioja, T., Morgunova, E., & Taipale, J. (2015). DNA-dependent formation of transcription factor pairs alters their binding specificity. *Nature*, *527*(7578), 384–388. https://doi.org/10.1038/nature15518

Junion, G., Spivakov, M., Girardot, C., Braun, M., Gustafson, E. H., Birney, E., & Furlong, E. E. (2012). A transcription factor collective defines cardiac cell fate and reflects lineage history. *Cell*, *148*(3), 473–486. https://doi.org/10.1016/j.cell.2012.01.030

Kaikkonen, M. U., Spann, N. J., Heinz, S., Romanoski, C. E., Allison, K. A., Stender, J. D., Chun, H. B., Tough, D. F., Prinjha, R. K., Benner, C., & Glass, C. K. (2013). Remodeling of

the enhancer landscape during macrophage activation is coupled to enhancer transcription. *Molecular Cell*, *51*(3), 310–325. https://doi.org/10.1016/j.molcel.2013.07.010

Kasowski, M., Grubert, F., Heffelfinger, C., Hariharan, M., Asabere, A., Waszak, S. M., Habegger, L., Rozowsky, J., Shi, M., Urban, A. E., Hong, M. Y., Karczewski, K. J., Huber, W., Weissman, S. M., Gerstein, M. B., Korbel, J. O., & Snyder, M. (2010). Variation in transcription factor binding among humans. *Science (New York, N.Y.)*, *328*(5975), 232–235. https://doi.org/10.1126/science.1183621

Keane, T. M., Goodstadt, L., Danecek, P., White, M. A., Wong, K., Yalcin, B., Heger, A., Agam, A., Slater, G., Goodson, M., Furlotte, N. A., Eskin, E., Nellåker, C., Whitley, H., Cleak, J., Janowitz, D., Hernandez-Pliego, P., Edwards, A., Belgard, T. G., Oliver, P. L., … Adams, D. J. (2011). Mouse genomic variation and its effect on phenotypes and gene regulation. *Nature*, *477*(7364), 289–294. https://doi.org/10.1038/nature10413

Keilwagen, J., Posch, S., & Grau, J. (2019). Accurate prediction of cell type-specific transcription factor binding. *Genome Biology*, *20*(1), 9. https://doi.org/10.1186/s13059-018-1614-y

Kilpinen, H., Waszak, S. M., Gschwind, A. R., Raghav, S. K., Witwicki, R. M., Orioli, A., Migliavacca, E., Wiederkehr, M., Gutierrez-Arcelus, M., Panousis, N. I., Yurovsky, A., Lappalainen, T., Romano-Palumbo, L., Planchon, A., Bielser, D., Bryois, J., Padioleau, I., Udin, G., Thurnheer, S., Hacker, D., … Dermitzakis, E. T. (2013). Coordinated effects of sequence variation on DNA binding, chromatin structure, and transcription. *Science (New York, N.Y.)*, *342*(6159), 744–747. https://doi.org/10.1126/science.1242463

Kim, T. H., Abdullaev, Z. K., Smith, A. D., Ching, K. A., Loukinov, D. I., Green, R. D., Zhang, M. Q., Lobanenkov, V. V., & Ren, B. (2007). Analysis of the vertebrate insulator protein CTCF-binding sites in the human genome. *Cell*, *128*(6), 1231–1245. https://doi.org/10.1016/j.cell.2006.12.048

Kim, T. K., Hemberg, M., Gray, J. M., Costa, A. M., Bear, D. M., Wu, J., Harmin, D. A., Laptewicz, M., Barbara-Haley, K., Kuersten, S., Markenscoff-Papadimitriou, E., Kuhl, D., Bito, H., Worley, P. F., Kreiman, G., & Greenberg, M. E. (2010). Widespread transcription at neuronal activity-regulated enhancers. *Nature*, *465*(7295), 182–187. https://doi.org/10.1038/nature09033

Kim, T. K., & Shiekhattar, R. (2015). Architectural and Functional Commonalities between Enhancers and Promoters. *Cell*, *162*(5), 948–959. https://doi.org/10.1016/j.cell.2015.08.008

King, D. M., Hong, C., Shepherdson, J. L., Granas, D. M., Maricque, B. B., & Cohen, B. A. (2020). Synthetic and genomic regulatory elements reveal aspects of *cis*-regulatory grammar in mouse embryonic stem cells. *eLife*, *9*, e41279. https://doi.org/10.7554/eLife.41279

Kharchenko, P. V., Tolstorukov, M. Y., & Park, P. J. (2008). Design and analysis of ChIP-seq experiments for DNA-binding proteins. *Nature Biotechnology*, *26*(12), 1351–1359. https://doi.org/10.1038/nbt.1508

Klein, J. C., Agarwal, V., Inoue, F., Keith, A., Martin, B., Kircher, M., Ahituv, N., & Shendure, J. (2020). A systematic evaluation of the design and context dependencies of massively parallel reporter assays. *Nature Methods*, *17*(11), 1083–1091. https://doi.org/10.1038/s41592-020-0965-y

Kribelbauer, J. F., Rastogi, C., Bussemaker, H. J., & Mann, R. S. (2019). Low-Affinity Binding Sites and the Transcription Factor Specificity Paradox in Eukaryotes. *Annual Review of Cell and Developmental Biology*, *35*, 357–379. https://doi.org/10.1146/annurev-cellbio-100617-062719

Kundaje, A., Meuleman, W., Ernst, J., Bilenky, M., Yen, A., Heravi-Moussavi, A., Kheradpour, P., Zhang, Z., Wang, J., Ziller, M. J., Amin, V., Whitaker, J. W., Schultz, M. D., Ward, L. D., Sarkar, A., Quon, G., Sandstrom, R. S., Eaton, M. L., Wu, Y. C., … Kellis, M. (2015). Integrative analysis of 111 reference human epigenomes. *Nature*, *518*(7539), 317–330. https://doi.org/10.1038/nature14248

Lappalainen T. (2015). Functional genomics bridges the gap between quantitative genetics and molecular biology. *Genome Research*, *25*(10), 1427–1431. https://doi.org/10.1101/gr.190983.115

Landt, S. G., Marinov, G. K., Kundaje, A., Kheradpour, P., Pauli, F., Batzoglou, S., Bernstein, B. E., Bickel, P., Brown, J. B., Cayting, P., Chen, Y., DeSalvo, G., Epstein, C., Fisher-Aylor, K. I., Euskirchen, G., Gerstein, M., Gertz, J., Hartemink, A. J., Hoffman, M. M., Iyer, V. R., … Snyder, M. (2012). ChIP-seq guidelines and practices of the ENCODE and modENCODE consortia. *Genome Research*, *22*(9), 1813–1831. https://doi.org/10.1101/gr.136184.111

Langmead, B., & Salzberg, S. L. (2012). Fast gapped-read alignment with Bowtie 2. *Nature Methods*, *9*(4), 357–359. https://doi.org/10.1038/nmeth.1923

Lappalainen, T., & MacArthur, D. G. (2021). From variant to function in human disease genetics. *Science (New York, N.Y.)*, *373*(6562), 1464–1468. https://doi.org/10.1126/science.abi8207

Lareau, C. A., & Aryee, M. J. (2018). hichipper: a preprocessing pipeline for calling DNA loops from HiChIP data. *Nature Methods*, *15*(3), 155–156. https://doi.org/10.1038/nmeth.4583

Leonard, D. A., & Kerppola, T. K. (1998). DNA bending determines Fos-Jun heterodimer orientation. *Nature Structural Biology*, *5*(10), 877–881. https://doi.org/10.1038/2316

Levo, M., & Segal, E. (2014). In pursuit of design principles of regulatory sequences. *Nature Reviews. Genetics*, *15*(7), 453–468. https://doi.org/10.1038/nrg3684

Li, H., Handsaker, B., Wysoker, A., Fennell, T., Ruan, J., Homer, N., Marth, G., Abecasis, G., Durbin, R., & 1000 Genome Project Data Processing Subgroup (2009). The Sequence Alignment/Map format and SAMtools. *Bioinformatics (Oxford, England)*, *25*(16), 2078–2079. https://doi.org/10.1093/bioinformatics/btp352

Li, Q. V., Dixon, G., Verma, N., Rosen, B. P., Gordillo, M., Luo, R., Xu, C., Wang, Q., Soh, C. L., Yang, D., Crespo, M., Shukla, A., Xiang, Q., Dündar, F., Zumbo, P., Witkin, M., Koche, R., Betel, D., Chen, S., Massagué, J., … Huangfu, D. (2019). Genome-scale screens identify JNK-JUN signaling as a barrier for pluripotency exit and endoderm differentiation. Nature Genetics, 51(6), 999–1010. https://doi.org/10.1038/s41588-019-0408-9

Li, Y. I., van de Geijn, B., Raj, A., Knowles, D. A., Petti, A. A., Golan, D., Gilad, Y., & Pritchard, J. K. (2016). RNA splicing is a primary link between genetic variation and disease. *Science (New York, N.Y.)*, *352*(6285), 600–604. https://doi.org/10.1126/science.aad9417

Lidor Nili, E., Field, Y., Lubling, Y., Widom, J., Oren, M., & Segal, E. (2010). p53 binds preferentially to genomic regions with high DNA-encoded nucleosome occupancy. *Genome Research*, *20*(10), 1361–1368. https://doi.org/10.1101/gr.103945.109

Liu T. (2014). Use model-based Analysis of ChIP-Seq (MACS) to analyze short reads generated by sequencing protein-DNA interactions in embryonic stem cells. *Methods in Molecular Biology (Clifton, N.J.)*, *1150*, 81–95. https://doi.org/10.1007/978-1-4939-0512-6_4

Liu, X., Li, H., Rajurkar, M., Li, Q., Cotton, J. L., Ou, J., Zhu, L. J., Goel, H. L., Mercurio, A. M., Park, J. S., Davis, R. J., & Mao, J. (2016). Tead and AP1 Coordinate Transcription and Motility. *Cell Reports*, *14*(5), 1169–1180. https://doi.org/10.1016/j.celrep.2015.12.104

Liao, Y., Smyth, G. K., & Shi, W. (2013). The Subread aligner: fast, accurate and scalable read mapping by seed-and-vote. *Nucleic Acids Research*, *41*(10), e108. https://doi.org/10.1093/nar/gkt214

Link, V. M., Duttke, S. H., Chun, H. B., Holtman, I. R., Westin, E., Hoeksema, M. A., Abe, Y., Skola, D., Romanoski, C. E., Tao, J., Fonseca, G. J., Troutman, T. D., Spann, N. J., Strid, T., Sakai, M., Yu, M., Hu, R., Fang, R., Metzler, D., Ren, B., … Glass, C. K. (2018). Analysis of Genetically Diverse Macrophages Reveals Local and Domain-wide Mechanisms that Control Transcription Factor Binding and Function. *Cell*, *173*(7), 1796–1809.e17. https://doi.org/10.1016/j.cell.2018.04.018

Long, H. K., Prescott, S. L., & Wysocka, J. (2016). Ever-Changing Landscapes: Transcriptional Enhancers in Development and Evolution. *Cell*, *167*(5), 1170–1187. https://doi.org/10.1016/j.cell.2016.09.018

Love, M. I., Huber, W., & Anders, S. (2014). Moderated estimation of fold change and dispersion for RNA-seq data with DESeq2. *Genome Biology*, *15*(12), 550. https://doi.org/10.1186/s13059-014-0550-8

Malik, A. N., Vierbuchen, T., Hemberg, M., Rubin, A. A., Ling, E., Couch, C. H., Stroud, H., Spiegel, I., Farh, K. K., Harmin, D. A., & Greenberg, M. E. (2014). Genome-wide identification and characterization of functional neuronal activity-dependent enhancers. *Nature Neuroscience*, *17*(10), 1330–1339. https://doi.org/10.1038/nn.3808

Maurano, M. T., Humbert, R., Rynes, E., Thurman, R. E., Haugen, E., Wang, H., Reynolds, A. P., Sandstrom, R., Qu, H., Brody, J., Shafer, A., Neri, F., Lee, K., Kutyavin, T., Stehling-Sun, S., Johnson, A. K., Canfield, T. K., Giste, E., Diegel, M., Bates, D., … Stamatoyannopoulos, J. A. (2012). Systematic localization of common disease-associated variation in regulatory DNA. *Science (New York, N.Y.)*, *337*(6099), 1190–1195. https://doi.org/10.1126/science.1222794

Maurano, M. T., Haugen, E., Sandstrom, R., Vierstra, J., Shafer, A., Kaul, R., & Stamatoyannopoulos, J. A. (2015). Large-scale identification of sequence variants influencing human transcription factor occupancy in vivo. *Nature Genetics*, *47*(12), 1393–1401. https://doi.org/10.1038/ng.3432

Meuleman, W., Muratov, A., Rynes, E., Halow, J., Lee, K., Bates, D., Diegel, M., Dunn, D., Neri, F., Teodosiadis, A., Reynolds, A., Haugen, E., Nelson, J., Johnson, A., Frerker, M., Buckley, M., Sandstrom, R., Vierstra, J., Kaul, R., & Stamatoyannopoulos, J. (2020). Index and biological spectrum of human DNase I hypersensitive sites. *Nature*, *584*(7820), 244–251. https://doi.org/10.1038/s41586-020-2559-3

Michael, A. K., & Thomä, N. H. (2021). Reading the chromatinized genome. *Cell*, *184*(14), 3599–3611. https://doi.org/10.1016/j.cell.2021.05.029

Miller, J. A., & Widom, J. (2003). Collaborative competition mechanism for gene activation in vivo. *Molecular and Cellular Biology*, *23*(5), 1623–1632. https://doi.org/10.1128/MCB.23.5.1623-1632.2003

Moyle-Heyrman, G., Tims, H. S., & Widom, J. (2011). Structural constraints in collaborative competition of transcription factors against the nucleosome. *Journal of Molecular Biology*, *412*(4), 634–646. https://doi.org/10.1016/j.jmb.2011.07.032

Mumbach, M. R., Satpathy, A. T., Boyle, E. A., Dai, C., Gowen, B. G., Cho, S. W., Nguyen, M. L., Rubin, A. J., Granja, J. M., Kazane, K. R., Wei, Y., Nguyen, T., Greenside, P. G., Corces, M. R., Tycko, J., Simeonov, D. R., Suliman, N., Li, R., Xu, J., Flynn, R. A., … Chang, H. Y. (2017). Enhancer connectome in primary human cells identifies target genes of disease-associated DNA elements. *Nature Genetics*, *49*(11), 1602–1612. https://doi.org/10.1038/ng.3963

Nasser, J., Bergman, D. T., Fulco, C. P., Guckelberger, P., Doughty, B. R., Patwardhan, T. A., Jones, T. R., Nguyen, T. H., Ulirsch, J. C., Lekschas, F., Mualim, K., Natri, H. M., Weeks, E. M., Munson, G., Kane, M., Kang, H. Y., Cui, A., Ray, J. P., Eisenhaure, T. M., Collins, R. L., … Engreitz, J. M. (2021). Genome-wide enhancer maps link risk variants to disease genes. *Nature*, *593*(7858), 238–243. https://doi.org/10.1038/s41586-021-03446-x

Osterwalder, M., Barozzi, I., Tissières, V., Fukuda-Yuzawa, Y., Mannion, B. J., Afzal, S. Y., Lee, E. A., Zhu, Y., Plajzer-Frick, I., Pickle, C. S., Kato, M., Garvin, T. H., Pham, Q. T., Harrington, A. N., Akiyama, J. A., Afzal, V., Lopez-Rios, J., Dickel, D. E., Visel, A., & Pennacchio, L. A. (2018). Enhancer redundancy provides phenotypic robustness in mammalian development. *Nature*, *554*(7691), 239–243. https://doi.org/10.1038/nature25461

Ou, S., Su, W., Liao, Y., Chougule, K., Agda, J., Hellinga, A. J., Lugo, C., Elliott, T. A., Ware, D., Peterson, T., Jiang, N., Hirsch, C. N., & Hufford, M. B. (2019). Benchmarking transposable element annotation methods for creation of a streamlined, comprehensive pipeline. *Genome Biology*, *20*(1), 275. https://doi.org/10.1186/s13059-019-1905-y

Quinlan, A. R., & Hall, I. M. (2010). BEDTools: a flexible suite of utilities for comparing genomic features. *Bioinformatics (Oxford, England)*, *26*(6), 841–842. https://doi.org/10.1093/bioinformatics/btq033

Paakinaho, V., Presman, D. M., Ball, D. A., Johnson, T. A., Schiltz, R. L., Levitt, P., Mazza, D., Morisaki, T., Karpova, T. S., & Hager, G. L. (2017). Single-molecule analysis of steroid receptor and cofactor action in living cells. *Nature Communications*, *8*, 15896. https://doi.org/10.1038/ncomms15896

Pai, A. A., Pritchard, J. K., & Gilad, Y. (2015). The genetic and mechanistic basis for variation in gene regulation. *PLoS Genetics*, *11*(1), e1004857. https://doi.org/10.1371/journal.pgen.1004857

Park, J., Eisenbarth, D., Choi, W., Kim, H., Choi, C., Lee, D., & Lim, D. S. (2020). YAP and AP-1 Cooperate to Initiate Pancreatic Cancer Development from Ductal Cells in Mice. *Cancer Research*, *80*(21), 4768–4779. https://doi.org/10.1158/0008-5472.CAN-20-0907

Pickrell J. K. (2014). Joint analysis of functional genomic data and genome-wide association studies of 18 human traits. *American Journal of Human Genetics*, *94*(4), 559–573. https://doi.org/10.1016/j.ajhg.2014.03.004

Rada-Iglesias, A., Bajpai, R., Swigut, T., Brugmann, S. A., Flynn, R. A., & Wysocka, J. (2011). A unique chromatin signature uncovers early developmental enhancers in humans. *Nature*, *470*(7333), 279–283. https://doi.org/10.1038/nature09692

Rickels, R., Herz, H. M., Sze, C. C., Cao, K., Morgan, M. A., Collings, C. K., Gause, M., Takahashi, Y. H., Wang, L., Rendleman, E. J., Marshall, S. A., Krueger, A., Bartom, E. T., Piunti, A., Smith, E. R., Abshiru, N. A., Kelleher, N. L., Dorsett, D., & Shilatifard, A. (2017). Histone H3K4 monomethylation catalyzed by Trr and mammalian COMPASS-like proteins at enhancers is dispensable for development and viability. *Nature Genetics*, *49*(11), 1647–1653. https://doi.org/10.1038/ng.3965

Risse, G., Jooss, K., Neuberg, M., Brüller, H. J., & Müller, R. (1989). Asymmetrical recognition of the palindromic AP1 binding site (TRE) by Fos protein complexes. *The EMBO Journal*, *8*(12), 3825–3832.

Roberts, G. A., Ozkan, B., Gachulincová, I., O'Dwyer, M. R., Hall-Ponsele, E., Saxena, M., Robinson, P. J., & Soufi, A. (2021). Dissecting OCT4 defines the role of nucleosome binding in pluripotency. *Nature Cell Biology*, *23*(8), 834–845. https://doi.org/10.1038/s41556-021-00727-5

Rohs, R., Jin, X., West, S. M., Joshi, R., Honig, B., & Mann, R. S. (2010). Origins of specificity in protein-DNA recognition. *Annual Review of Biochemistry*, *79*, 233–269. https://doi.org/10.1146/annurev-biochem-060408-091030

Schmidt, D., Schwalie, P. C., Wilson, M. D., Ballester, B., Gonçalves, A., Kutter, C., Brown, G. D., Marshall, A., Flicek, P., & Odom, D. T. (2012). Waves of retrotransposon expansion remodel genome organization and CTCF binding in multiple mammalian lineages. *Cell*, *148*(1-2), 335–348. https://doi.org/10.1016/j.cell.2011.11.058

Seo, J., Koçak, D. D., Bartelt, L. C., Williams, C. A., Barrera, A., Gersbach, C. A., & Reddy, T. E. (2021). AP-1 subunits converge promiscuously at enhancers to potentiate transcription. *Genome Research*, *31*(4), 538–550. https://doi.org/10.1101/gr.267898.120

Servant, N., Varoquaux, N., Lajoie, B. R., Viara, E., Chen, C. J., Vert, J. P., Heard, E., Dekker, J., & Barillot, E. (2015). HiC-Pro: an optimized and flexible pipeline for Hi-C data processing. *Genome Biology*, *16*, 259. https://doi.org/10.1186/s13059-015-0831-x

Sharma, N., Pollina, E. A., Nagy, M. A., Yap, E. L., DiBiase, F. A., Hrvatin, S., Hu, L., Lin, C., & Greenberg, M. E. (2019). ARNT2 Tunes Activity-Dependent Gene Expression through NCoR2-Mediated Repression and NPAS4-Mediated Activation. *Neuron*, *102*(2), 390–406.e9. https://doi.org/10.1016/j.neuron.2019.02.007

Shen, S. Q., Turro, E., & Corbo, J. C. (2014). Hybrid mice reveal parent-of-origin and Cis- and trans-regulatory effects in the retina. *PloS One*, *9*(10), e109382. https://doi.org/10.1371/journal.pone.0109382

Shen, Z., Li, R. Z., Prohaska, T. A., Hoeksema, M. A., Spann, N. J., Tao, J., Fonseca, G. J., Le, T., Stolze, L., Sakai, M., Romanoski, C. E., & Glass, C. K. (2021). Systematic analysis of naturally occurring insertions and deletions that alter transcription factor spacing identifies tolerant and sensitive transcription factor pairs. *bioRxiv* 2020.04.02.021535; doi: https://doi.org/10.1101/2020.04.02.021535

Skene, P. J., & Henikoff, S. (2017). An efficient targeted nuclease strategy for high-resolution mapping of DNA binding sites. *eLife*, *6*, e21856. https://doi.org/10.7554/eLife.21856

Soufi, A., Garcia, M. F., Jaroszewicz, A., Osman, N., Pellegrini, M., & Zaret, K. S. (2015). Pioneer transcription factors target partial DNA motifs on nucleosomes to initiate reprogramming. *Cell*, *161*(3), 555–568. https://doi.org/10.1016/j.cell.2015.03.017

Spitz, F., & Furlong, E. E. (2012). Transcription factors: from enhancer binding to developmental control. *Nature Reviews. Genetics*, *13*(9), 613–626. https://doi.org/10.1038/nrg3207

Sun W. (2012). A statistical framework for eQTL mapping using RNA-seq data. *Biometrics*, *68*(1), 1–11. https://doi.org/10.1111/j.1541-0420.2011.01654.x

Tehranchi, A. K., Myrthil, M., Martin, T., Hie, B. L., Golan, D., & Fraser, H. B. (2016). Pooled ChIP-Seq Links Variation in Transcription Factor Binding to Complex Disease Risk. *Cell*, *165*(3), 730–741. https://doi.org/10.1016/j.cell.2016.03.041

Tillo, D., Kaplan, N., Moore, I. K., Fondufe-Mittendorf, Y., Gossett, A. J., Field, Y., Lieb, J. D., Widom, J., Segal, E., & Hughes, T. R. (2010). High nucleosome occupancy is encoded at human regulatory sequences. *PloS One*, *5*(2), e9129. https://doi.org/10.1371/journal.pone.0009129

van de Geijn, B., McVicker, G., Gilad, Y., & Pritchard, J. K. (2015). WASP: allele-specific software for robust molecular quantitative trait locus discovery. *Nature Methods*, *12*(11), 1061–1063. https://doi.org/10.1038/nmeth.3582

van der Veeken, J., Zhong, Y., Sharma, R., Mazutis, L., Dao, P., Pe'er, D., Leslie, C. S., & Rudensky, A. Y. (2019). Natural Genetic Variation Reveals Key Features of Epigenetic and Transcriptional Memory in Virus-Specific CD8 T Cells. *Immunity*, *50*(5), 1202–1217.e7. https://doi.org/10.1016/j.immuni.2019.03.031

VandenBosch, L. S., Luu, K., Timms, A. E., Challam, S., Wu, Y., Lee, A. Y., & Cherry, T. J. (2022). Machine Learning Prediction of Non-Coding Variant Impact in Human Retinal cis-Regulatory Elements. *Translational vision science & technology*, *11*(4), 16. https://doi.org/10.1167/tvst.11.4.16

Vierbuchen, T., Ling, E., Cowley, C. J., Couch, C. H., Wang, X., Harmin, D. A., Roberts, C., & Greenberg, M. E. (2017). AP-1 Transcription Factors and the BAF Complex Mediate Signal-Dependent Enhancer Selection. *Molecular Cell*, *68*(6), 1067–1082.e12. https://doi.org/10.1016/j.molcel.2017.11.026

Vierstra, J., Lazar, J., Sandstrom, R., Halow, J., Lee, K., Bates, D., Diegel, M., Dunn, D., Neri, F., Haugen, E., Rynes, E., Reynolds, A., Nelson, J., Johnson, A., Frerker, M., Buckley, M., Kaul, R., Meuleman, W., & Stamatoyannopoulos, J. A. (2020). Global reference mapping of human transcription factor footprints. *Nature*, *583*(7818), 729–736. https://doi.org/10.1038/s41586-020-2528-x

Villar, D., Berthelot, C., Aldridge, S., Rayner, T. F., Lukk, M., Pignatelli, M., Park, T. J., Deaville, R., Erichsen, J. T., Jasinska, A. J., Turner, J. M., Bertelsen, M. F., Murchison, E. P., Flicek, P., & Odom, D. T. (2015). Enhancer evolution across 20 mammalian species. *Cell*, *160*(3), 554–566. https://doi.org/10.1016/j.cell.2015.01.006

Wei, B., Jolma, A., Sahu, B., Orre, L. M., Zhong, F., Zhu, F., Kivioja, T., Sur, I., Lehtiö, J., Taipale, M., & Taipale, J. (2018). A protein activity assay to measure global transcription factor activity reveals determinants of chromatin accessibility. *Nature Biotechnology*, *36*(6), 521–529. https://doi.org/10.1038/nbt.4138

Wittkopp, P. J., & Kalay, G. (2011). Cis-regulatory elements: molecular mechanisms and evolutionary processes underlying divergence. *Nature Reviews. Genetics*, *13*(1), 59–69. https://doi.org/10.1038/nrg3095

Wong, E. S., Schmitt, B. M., Kazachenka, A., Thybert, D., Redmond, A., Connor, F., Rayner, T. F., Feig, C., Ferguson-Smith, A. C., Marioni, J. C., Odom, D. T., & Flicek, P. (2017). Interplay of cis and trans mechanisms driving transcription factor binding and gene expression evolution. *Nature Communications*, *8*(1), 1092. https://doi.org/10.1038/s41467-017-01037-x

Yella, V. R., Bhimsaria, D., Ghoshdastidar, D., Rodríguez-Martínez, J. A., Ansari, A. Z., & Bansal, M. (2018). Flexibility and structure of flanking DNA impact transcription factor affinity for its core motif. *Nucleic Acids Research*, *46*(22), 11883–11897. https://doi.org/10.1093/nar/gky1057

Zanconato, F., Forcato, M., Battilana, G., Azzolin, L., Quaranta, E., Bodega, B., Rosato, A., Bicciato, S., Cordenonsi, M., & Piccolo, S. (2015). Genome-wide association between YAP/TAZ/TEAD and AP-1 at enhancers drives oncogenic growth. *Nature Cell Biology*, *17*(9), 1218–1227. https://doi.org/10.1038/ncb3216

Zeitlinger J. (2020). Seven myths of how transcription factors read the cis-regulatory code. *Current Opinion in Systems Biology*, *23*, 22–31. https://doi.org/10.1016/j.coisb.2020.08.002

Zhou, K., Gaullier, G., & Luger, K. (2019). Nucleosome structure and dynamics are coming of age. *Nature Structural & Molecular Biology*, *26*(1), 3–13. https://doi.org/10.1038/s41594-018-0166-x

Zhu, F., Farnung, L., Kaasinen, E., Sahu, B., Yin, Y., Wei, B., Dodonova, S. O., Nitta, K. R., Morgunova, E., Taipale, M., Cramer, P., & Taipale, J. (2018). The interaction landscape between transcription factors and the nucleosome. *Nature*, *562*(7725), 76–81. https://doi.org/10.1038/s41586-018-0549-5

Zhu, Q., Liu, N., Orkin, S. H., & Yuan, G. C. (2019). CUT&RUNTools: a flexible pipeline for CUT&RUN processing and footprint analysis. *Genome Biology*, *20*(1), 192. https://doi.org/10.1186/s13059-019-1802-4

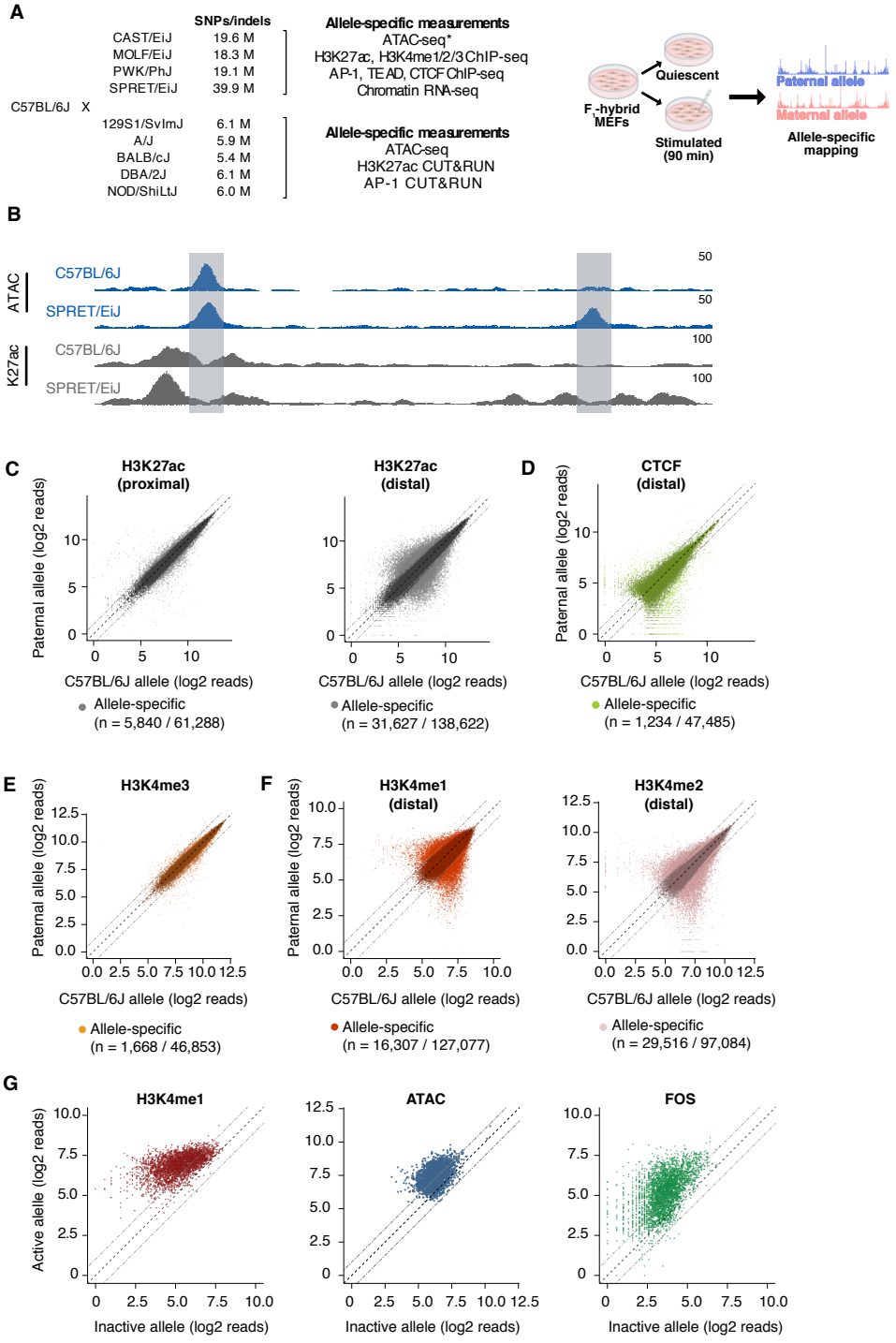

Figure 1. Allele-speciifc mapping of CREs and TF binding.

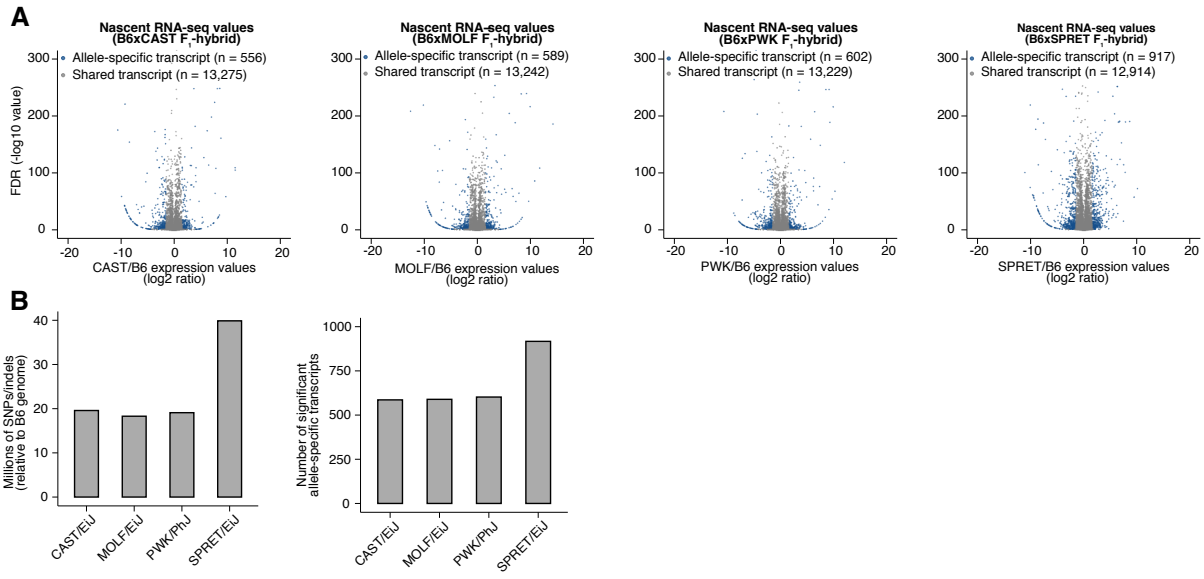

Figure 1 -- figure supplement 1. Identification of allele-specific transcripts using chromatin-associated RNA-seq.

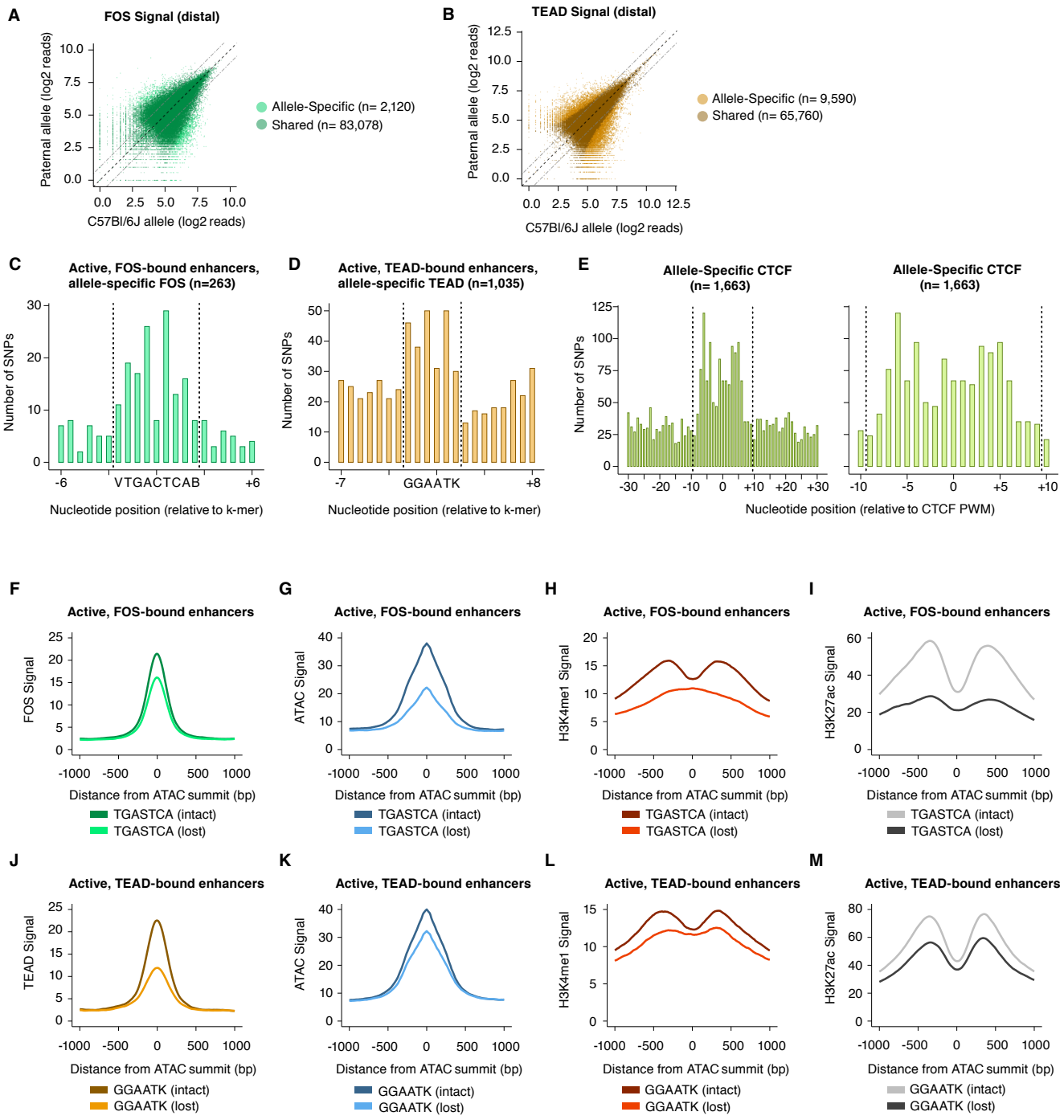

Figure 3. Sequence motifs and changes in chromatin state at allele-specific TF-bound sites.

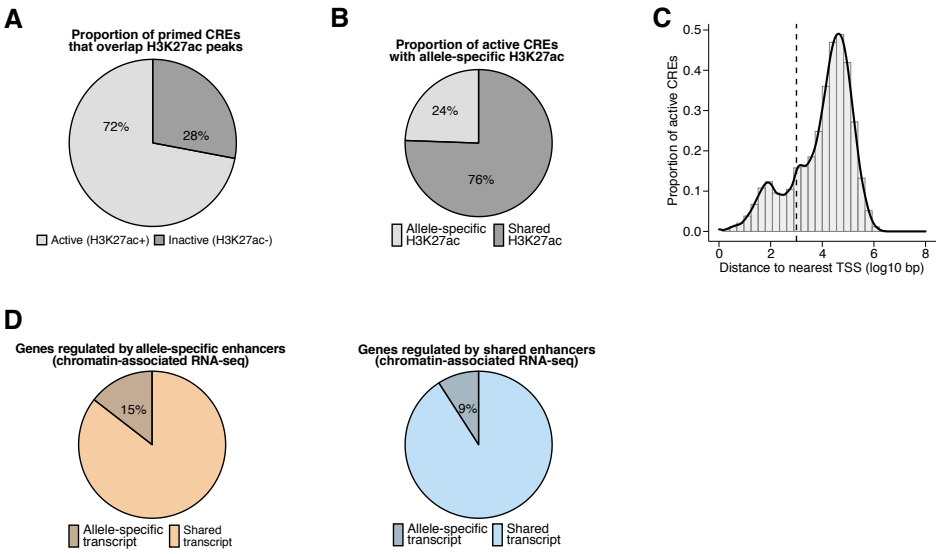

Figure 1 -- figure supplement 2. Properties of allele-specific enhancers and association with gene expression.

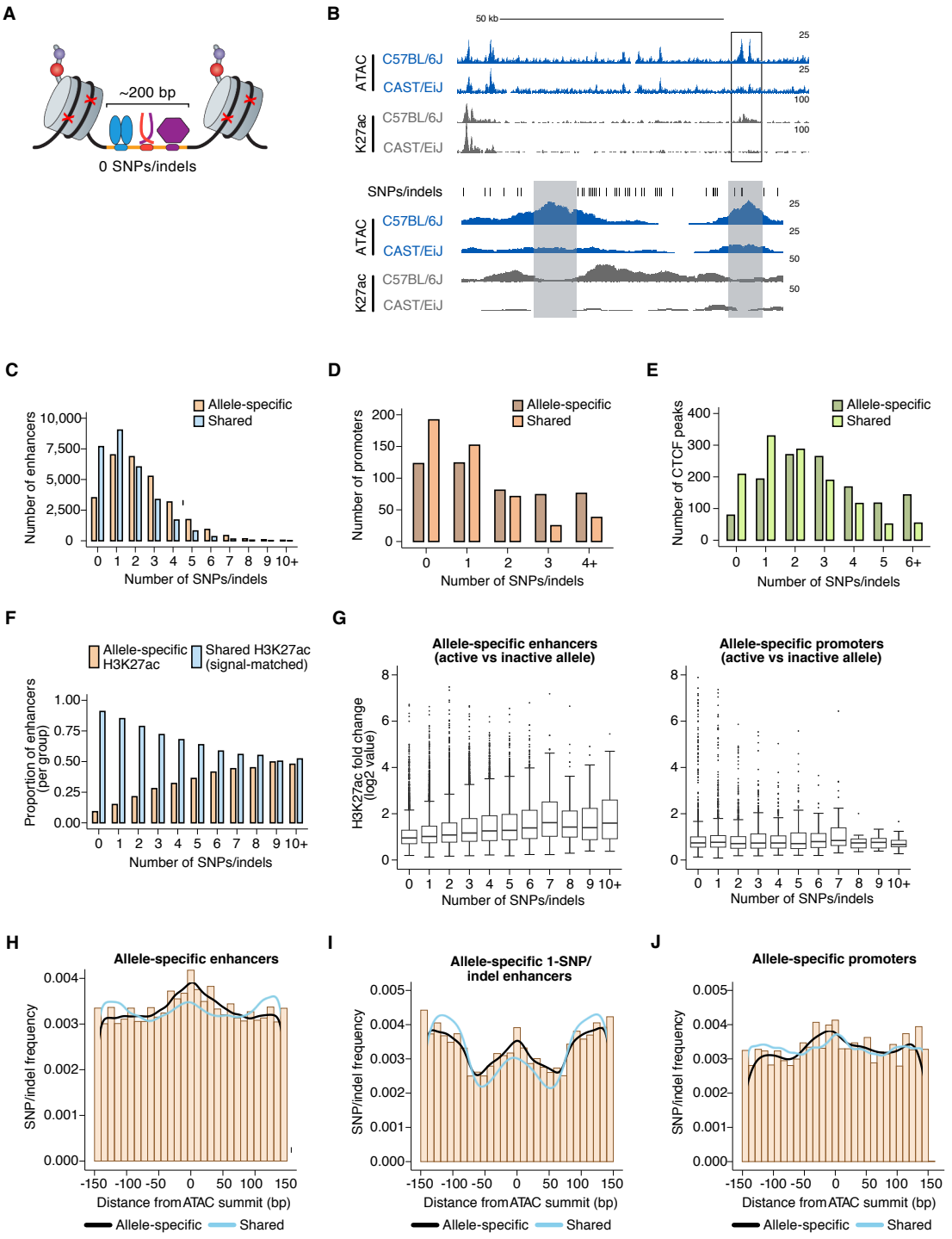

Figure 2. Number and position of sequence variants at allele-specific CREs.

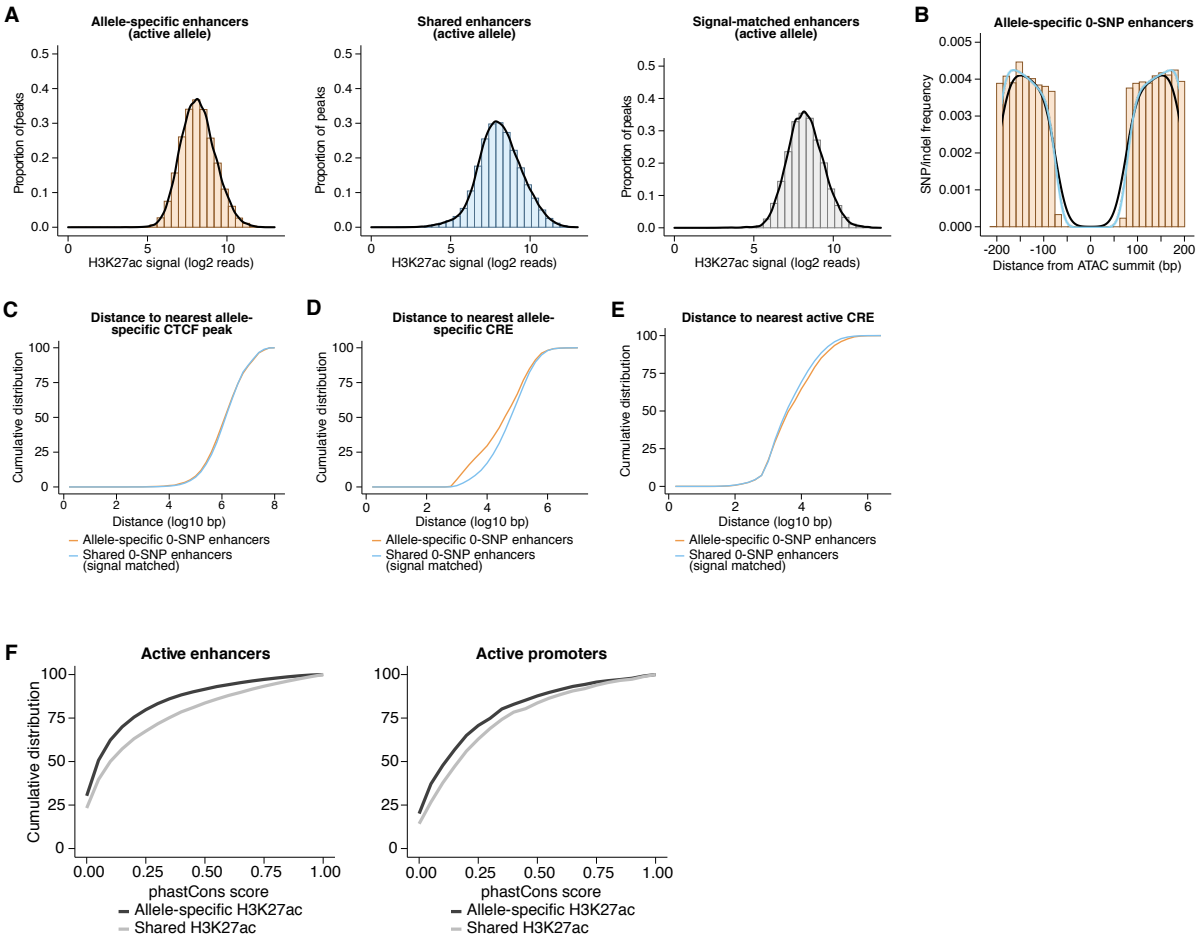

Figure 2 -- figure supplement 1. Contribution of locus-scale, *cis*-acting mechanisms to enhancer activity.

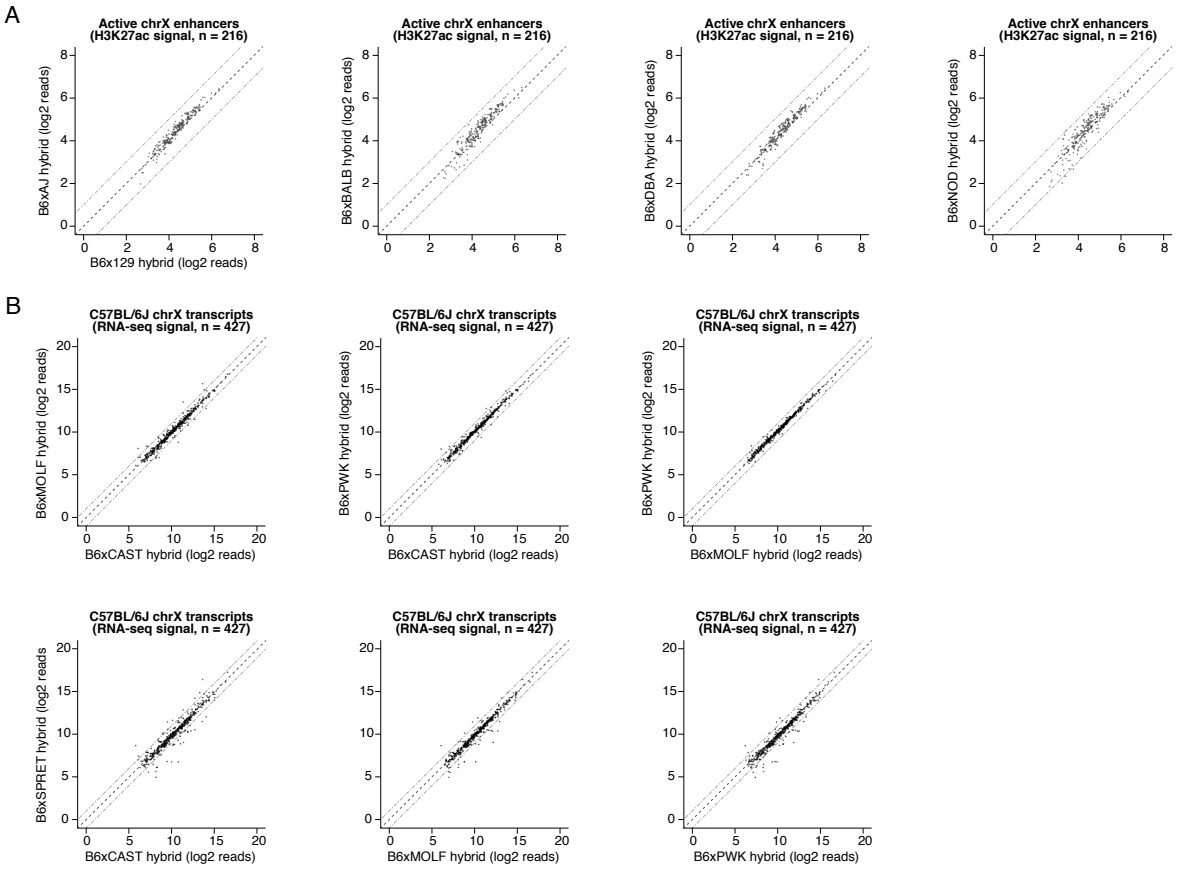

Figure 2 -- figure supplement 2. Quantification of *trans*-acting effects on enhancer chromatin state and gene expression.

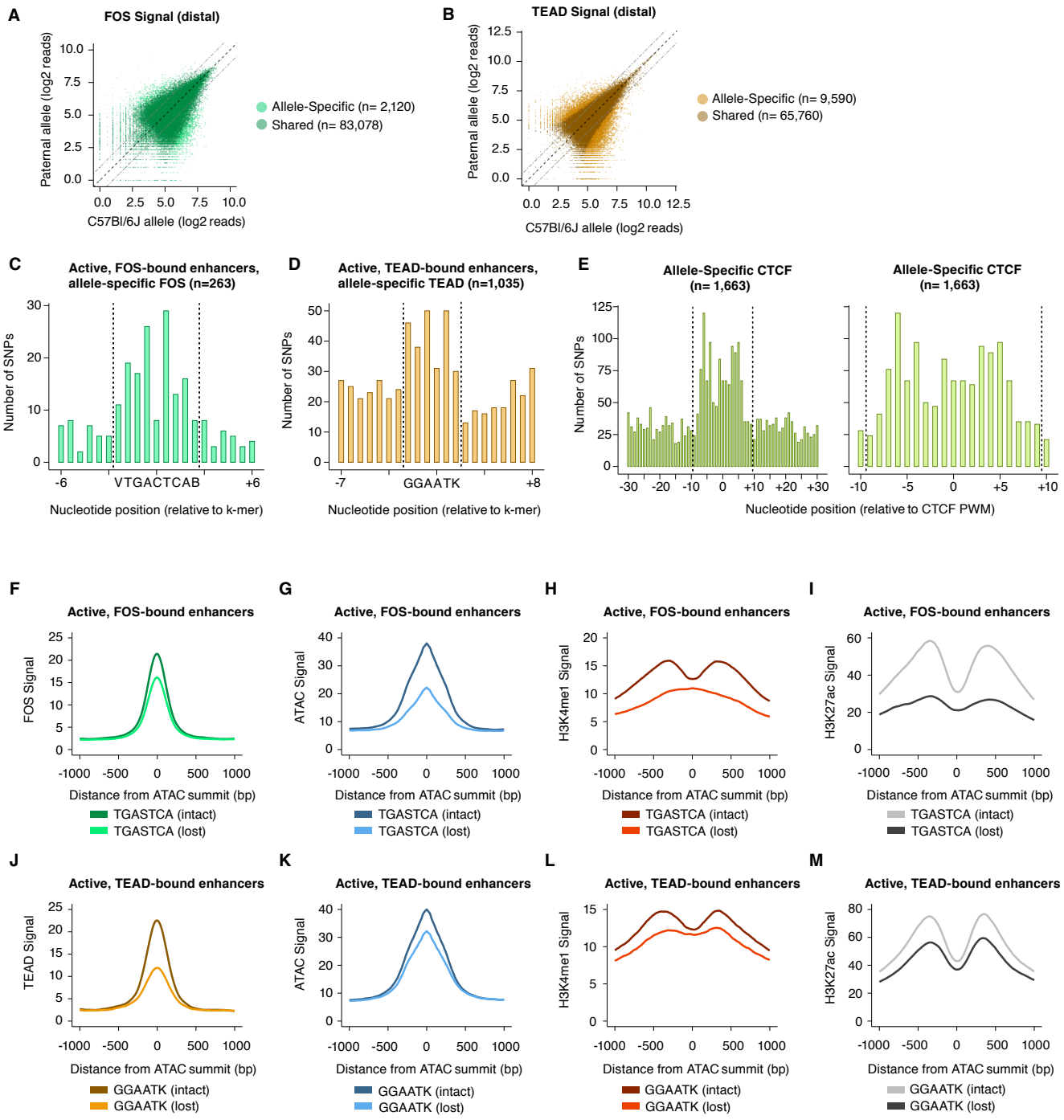

Figure 3. Sequence motifs and changes in chromatin state at allele-specific TF-bound sites.

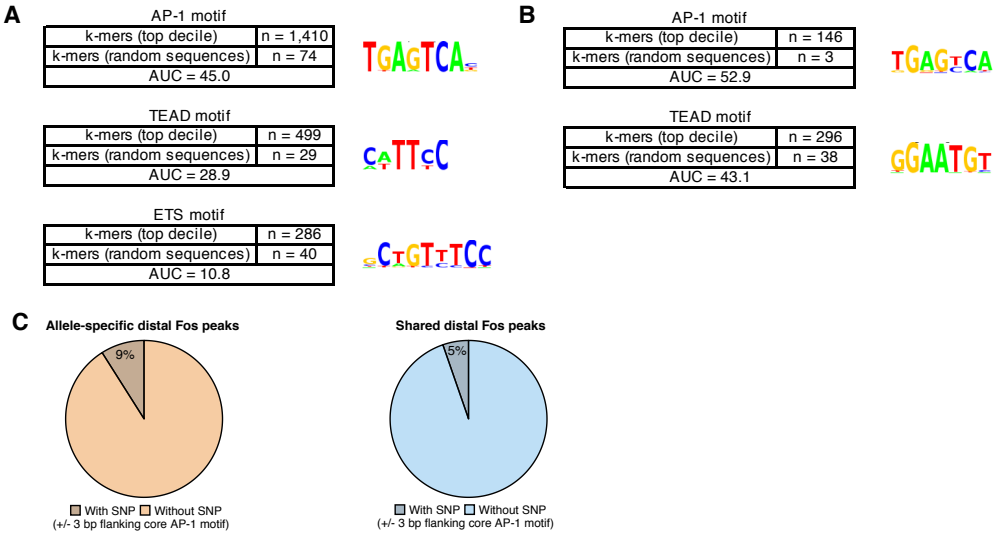

Figure 3 -- figure supplement 1. Sequence determinants of AP-1 binding.

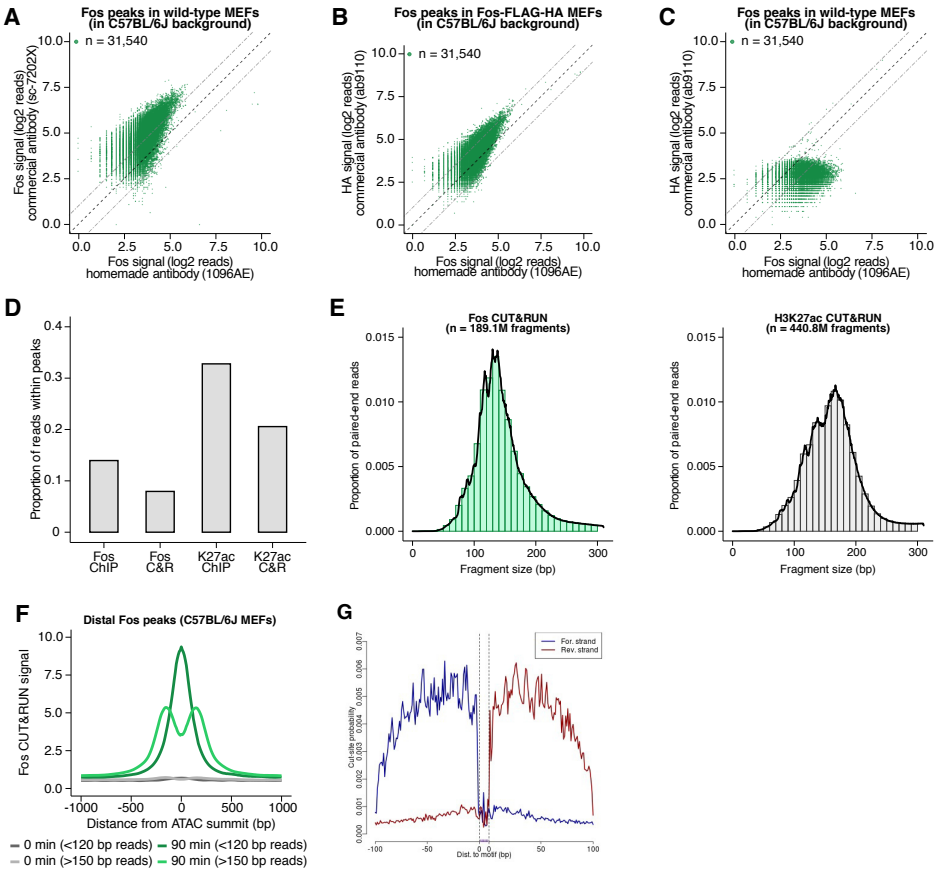

Figure 3 -- figure supplement 2. Comparison of ChIP-seq and CUT&RUN datasets.

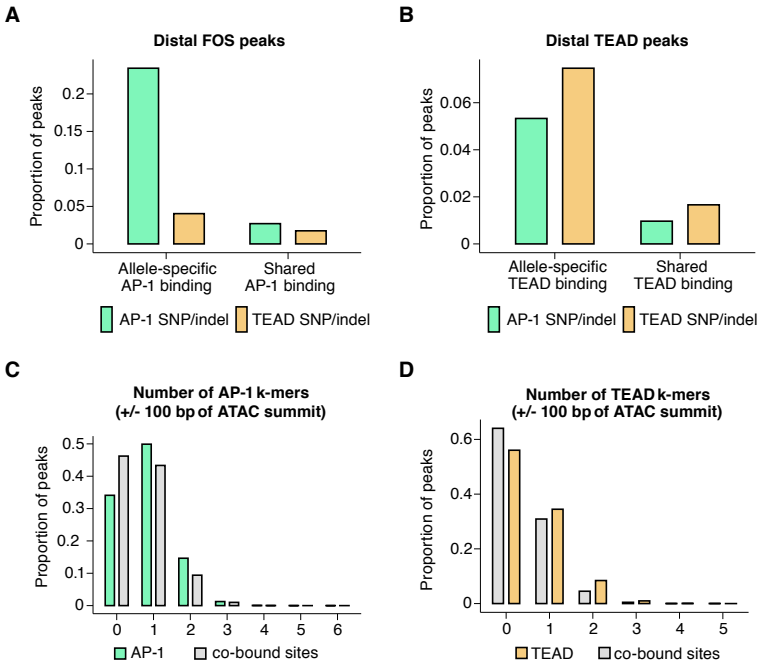

Figure 4. Mechanisms of hierarchical binding for AP-1 and TEAD TFs.

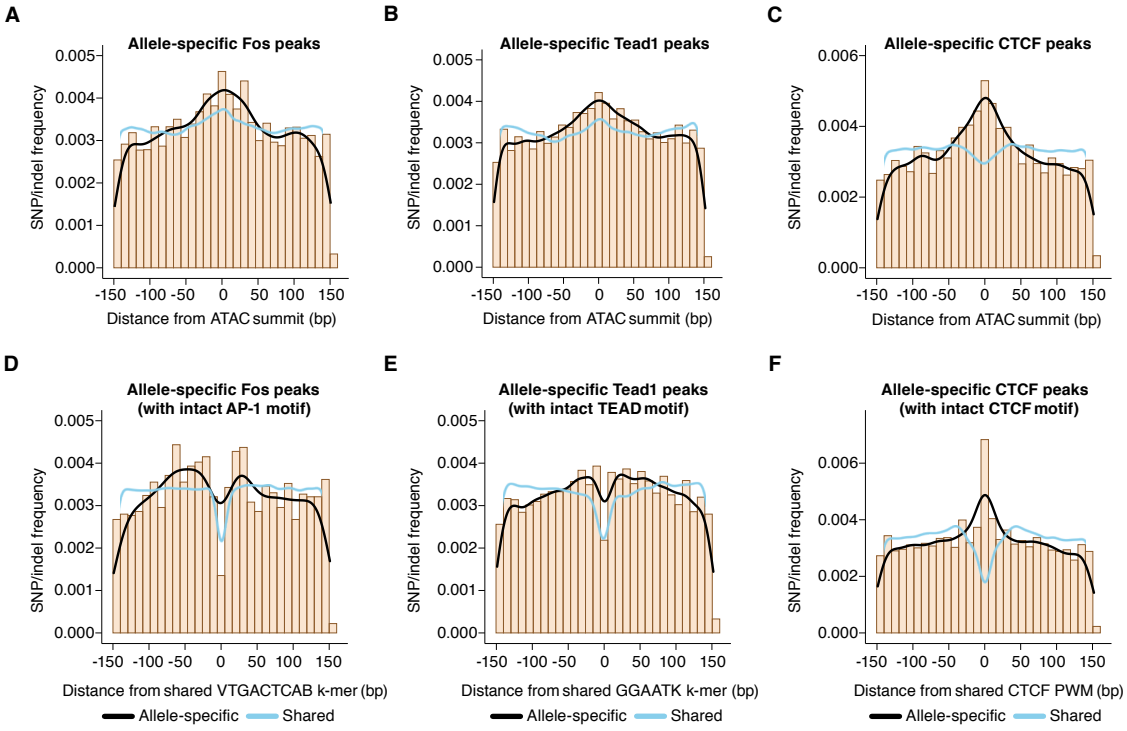

Figure 5. Distribution of sequence variants that influence AP-1, TEAD, and CTCF binding

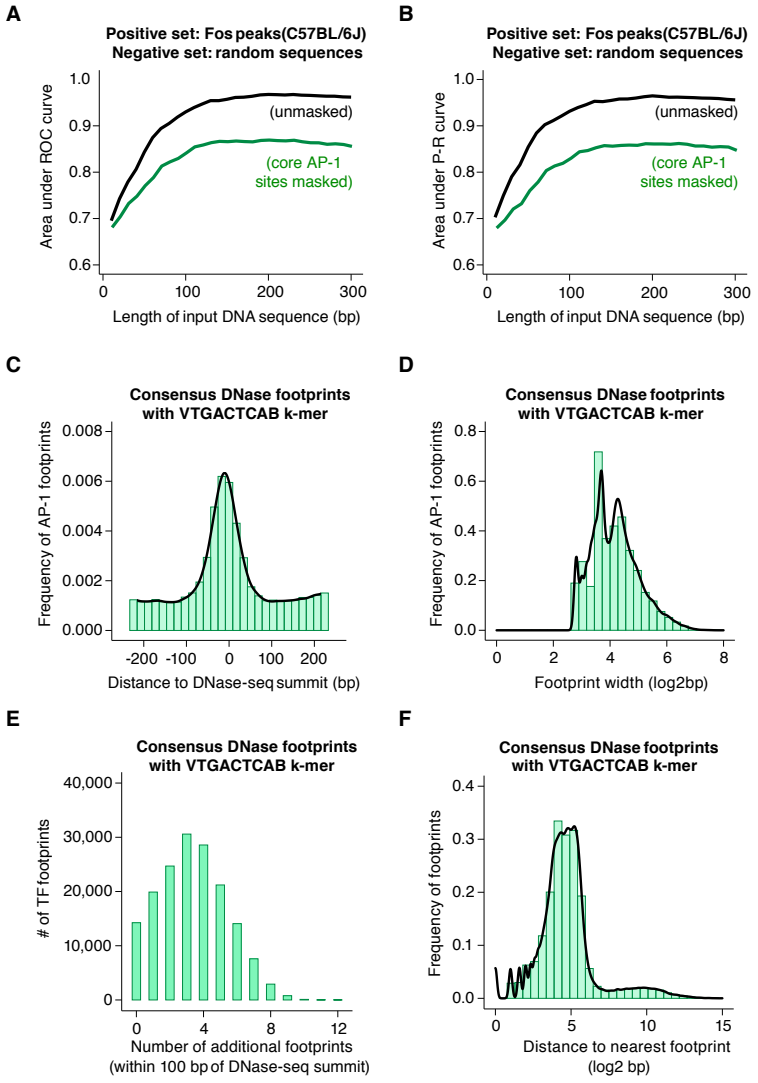

Figure 6. Machine learning prediction of AP-1 binding sites genome-wide.

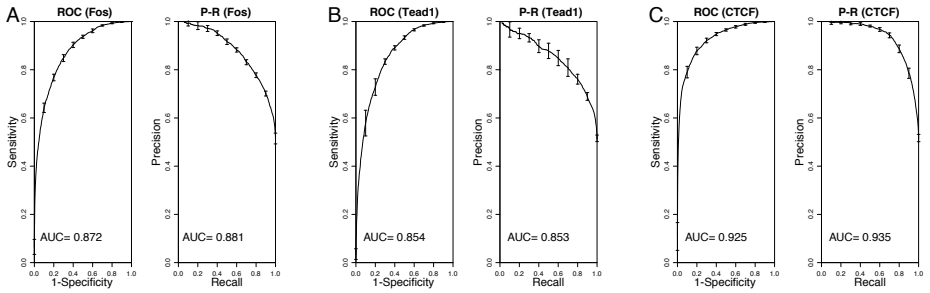

D **Fos peaks (C57BL/6J)**

AP-1 k-mers	
k-mer	Weight
TGAGTCATCA	2.689007
ATGAGTCATA	2.660156
TGAGTCATCA	2.615426
GA**TGAGTCA**C	2.519426
ATGAGTCACA	2.479271

E **Fos peaks (C57BL/6J) (core AP-1 sites masked)**

AP-1 k-mers	
k-mer	Weight
ATGAATCATA	1.785117
ATGATTCATC	1.736480
ATGAATCACA	1.704323
ATGATTCATA	1.664016
ATGATTCATG	1.639575

F **Tead1 peaks (C57BL/6J)**

AP-1 k-mers	
k-mer	Weight
ATGACTCATA	2.182203
AG**TGAGTCA**T	2.175822
ATGAGTCATC	2.153579
AA**TGAGTCA**T	2.131991
ATGAGTCACA	2.126289

G **CTCF peaks (C57BL/6J)**

CTCF k-mers	
k-mer	Weight
CCACCAGGGG	3.128552
CCACTAGGGG	3.034749
CACTAGAGGG	3.002243
CACCTGGTGG	2.854984
CCACTAGAGG	2.818653

H **Active Fos-bound allele**

AP-1 k-mers	
k-mer	Weight
CTA**TGACTCA**	1.247571
ATGACTCAGA	0.946615
ATGACTCAGC	0.929197
CTG**TGACTCA**	0.925876
CTC**TGACTCA**	0.890014

ETS k-mer	
k-mer	Weight
T**CTTCC**CACA	0.883873

Half AP-1 site	
k-mer	Weight
AGACAG**TGAC**	0.848271

I **VTGACTCAB footprints**

TEAD k-mer	
k-mer	Weight
GGAATTTCCA	1.301616

ETS k-mers	
k-mer	Weight
CA**GGAAG**TGG	1.316957
GGAAATTCCA	1.316957
TC**TAACC**ACA	1.316957

Half AP-1 site	
k-mer	Weight
TC**TGAC**CACA	1.717927

Figure 6 -- figure supplement 1. Application of the gkm-svm algorithm identifies k-mers required for AP-1, TEAD, and CTCF binding